Master Thesis
Industrial Engineering

Structural assessment of the ITER Fast-Ion Loss Detector

Author: Juan Carlos Rodríguez Criado
Supervisors: Juan Manuel Ayllón Guerola
Manuel Toscano Jiménez

Dep. Física Aplicada III
Escuela Técnica Superior de Ingeniería
University of Seville

Seville, 2018

Master Thesis
Industrial Engineering

Structural assessment of the ITER Fast-Ion Loss Detector

Author:
Juan Carlos Rodríguez Criado

Supervisor:
Juan Manuel Ayllón Guerola
Assistant Professor
Manuel Toscano Jiménez
Associate Professor

Dep. de Física Aplicada III
Escuela Técnica Superior de Ingeniería
University of Seville
Seville, 2018

Master Thesis: Structural assessment of the ITER Fast-Ion Loss Detector

Author: Juan Carlos Rodríguez Criado

Supervisor: Juan Manuel Ayllón Guerola
Manuel Toscano Jiménez

El tribunal nombrado para juzgar el Proyecto arriba indicado, compuesto por los siguientes miembros:

Presidente:

Vocales:

Secretario:

Acuerdan otorgarle la calificación de:

Sevilla, 2018

El Secretario del Tribunal

A mis padres
y Ainhoa
por su extraordinaria ayuda

Acknowledgment

Este trabajo no podría haberse realizado sin la colaboración de aquellas personas que han estado apoyándome durante el transcurso de este proyecto.

En primer lugar, agradecer a los directores de este proyecto por haberme ayudado todo lo posible. A Manuel por haberme dado la oportunidad y a Juanma por dirigirme, enseñarme y dar los consejos adecuados para poder terminar con éxito este trabajo.

No me puedo olvidar de mis compañeros de grado y máster, en especial Andrés, Antonio, Sergio Serrano y Sergio Moreno; por estar siempre apoyándonos mutuamente ante cualquier problema.

Por último, debo mencionar a aquellas personas que han sido un apoyo moral durante el proyecto. A toda mi familia por preocuparse de mi y por la evolución del proyecto; en especial a mis padres que me han dado su apoyo en cualquier aspecto profesional y personal.

Finalmente, dedicar una mención especial para Ainhoa que me acompaña en estos últimos e importantes años, apoyándome cuando las cosas salen mal y cuando salen bien; escuchándome y dándome consejos.

Gracias.

Juan Carlos Rodríguez Criado

Julio de 2018

Abstract

ITER is an experimental nuclear fusion reactor where the aim is to achieve a technology that provides clean, safe and unlimited energy. To reach this point it is necessary to study the plasma and the physical phenomena that occur during the fusion reaction, to finally be able to control the plasma and generate energy. Hence the experimental character of the reactor.

Diagnostic systems such as FILD (Fast-Ion Loss Detector) play an important role in understanding the fusion process. But the fact of being incorporated in this system means that it is exposed to certain loads, such as those generated by electromagnetic disruptions.

The main objective of this master thesis is to achieve a FILD design that is capable of resisting static loads due to electromagnetic disruptions, starting from an initial concept of the device.

To achieve this objective, a study of electromagnetic loads that act on FILD during a magnetic disruption is performed.

Simulations are carried out using a finite element model to make changes in the conceptual design and obtain a device that can resist these loads optimally.

Table of contents

LIST OF TABLES

LIST OF FIGURES

1 INTRODUCTION

1.1 Fusion energy

This is a difficult time for the energy industry. Many of the new signals emerging, disruptive digitalization, the commitment to decarbonization and desire, in some counties, for a more national focus; indicate that new frameworks for thinking are needed.

The period of 1970 to 2015 was one of remarkable world economic growth: The increase in the Gross World Product, the population, and the labour force, was complemented with a high rate of productivity growth; which led to an increase in energy demand [1].

According to a recent study by U.S. Energy Information Administration [2], world energy consumption will rise 28% between 2015 and 2040. Currently, most of the energy resources that provide energy to the planet are of natural origin, especially fossil fuels; while renewable energies remain in the background due to their low efficiency and dependence on climatic conditions. What happens with fission nuclear energy is the same because of the generation of radioactive and dangerous waste.

It is expected that in de coming years the consumption of renewable energies will increase, but so will fossil fuels, which is not sustainable due to the overexploitation of these resources, as well as the negative consequences on the environment. Global warming is a problem that is being addressed in key points of reports like World Energy Scenarios 2016 [1].

Given these arguments, there is a need to find a source of sustainable, safe, inexhaustible and clean energy. Nuclear fusion energy is a promising field in these aspects, but its developments as an energy source is one of the most complex scientific and technical tasks ever undertaken for non-military purposes and will still span several human generations [3].

The fusion reaction that is easiest to accomplish is the reaction between two hydrogen isotopes: deuterium, extracted from water and tritium, produced during the fusion reaction through contact with lithium. When deuterium and tritium nuclei fuse, they form a helium nucleus, a neutron and a lot of energy [4].

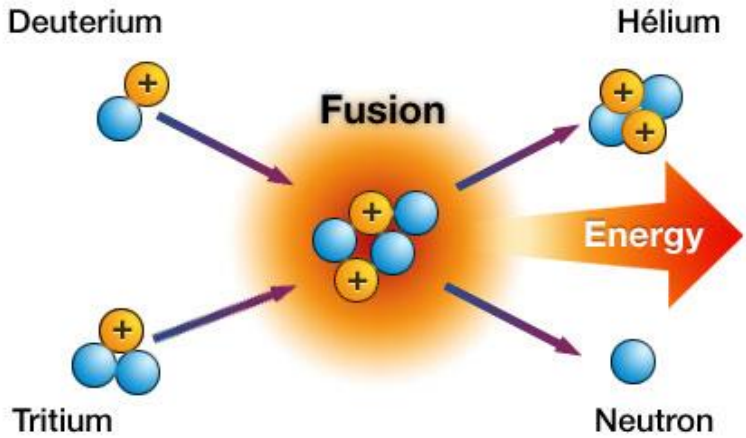

Figure 1: Nuclear fusion reaction

The kinetic energy released is due to the mass difference between reactants and products, according to the Einstein formula ($E = \Delta m \cdot c^2$) that can be used to generate electricity. This is the reason why so little fuel can produce so much energy: When burnt in a fusion reactor, the deuterium contained in 1 L of water (about 33 mg) will produce as much energy as burning 260 L of gasoline [3].

Since 1991 several megawatts of fusion power have been released in a controlled way in deuterium-tritium experiments in JET (Joint European Torus, Culham, UK) and TFTR (Tokamak Fusion Test Reactor, Princeton, USA) [3]. These experiments are carried out in nuclear fusion reactors of tokamak type (most widespread). The tokamak is a toroidal plasma confinement system, the plasma being confined by a magnetic field. The principal magnetic field is the toroidal field. However, this field alone does not allow confinement of the plasma, it is necessary a poloidal magnetic field [5].

This Master Thesis is framed in ITER (International Thermonuclear Experimental Reactor). ITER is one of the most ambitious energy projects today. In southern France (Cadarache), 35 nations are collaborating to build the world's largest tokamak, a magnetic fusion device that has been designed to prove the feasibility of fusion as a large-scale and carbon-free source of energy based on the same principle that powers our Sun and stars. In figure 2, a rendering of the complex where the reactor is installed is shown.

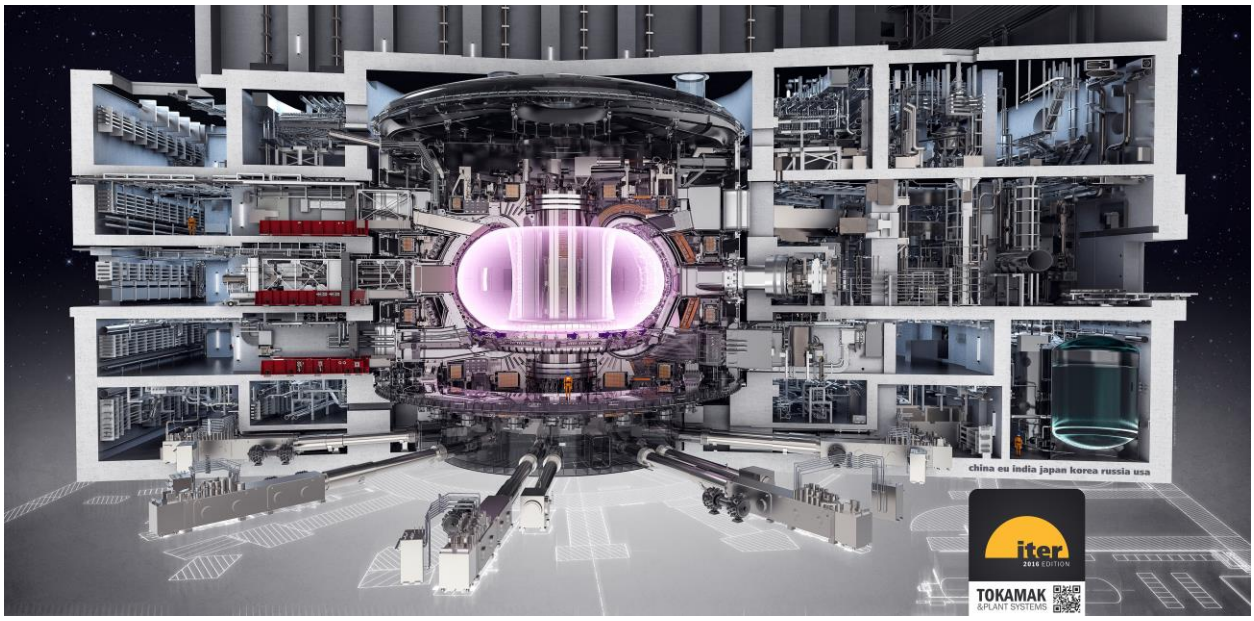

Figure 2: ITER scheme

ITER is designed to produce a ten-fold return of energy (Q = 10), or 500 MW of fusion power from 50 MW of input heating power. ITER will not capture the energy it produces as electricity, but -as first of all fusion experiments in history to produce net energy gain- it will prepare the way for the machine that can [6].

Other objectives can be summarized in:

- Demonstrate the integrated operation of technologies for a fusion power plant. Scientist will be able to study plasmas under conditions similar to those expected in a future power plant and test technologies such as heating, control, diagnostics, cryogenics and remote maintenance.
- Achieve a deuterium-tritium plasma in which the reaction is sustained through internal heating. Scientists are confident that the plasmas in ITER will not only produce much more fusion energy but will remain stable for longer periods of time.
- Test tritium breeding. The world supply of tritium is not sufficient to cover the needs of future power plants. ITER will provide a unique opportunity to test mockup in-vessel tritium breeding blankets in a real fusion environment.
- Demonstrate the safety characteristics of a fusion device. One of the primary goals of ITER operation is to demonstrate the control of the plasma and the fusion reactions with negligible consequences to the environment.

1.2 The Fast-Ion Loss Detector (FILD)

In ITER, fusion reactions and the use of various specific systems such as ion cyclotron heating and neutral beam injection can generate fast ions. Fast-ions are the population of ions whose energy is above the thermal energy, i.e. the bulk plasma energy. Therefore, they can be expelled from the core region to plasma edge by various instabilities. Even though they are a small fraction of the total ions population, they have a crucial effect on fusion devices performance and plasma stability because of their high energy [7].

The Fast-Ion Loss Detector (FILD) is one of the most widely used diagnostic for measuring fast ions in the plasma edge (Figure 3). A fraction of the incident fast ions is transmitted into a FILD where they encounter a scintillator and/or an array of Faraday cups. The interaction of fast ions with the scintillator provides measurements of their energy and the velocity pitch. This permits extracting information about the underlying loss process [8].

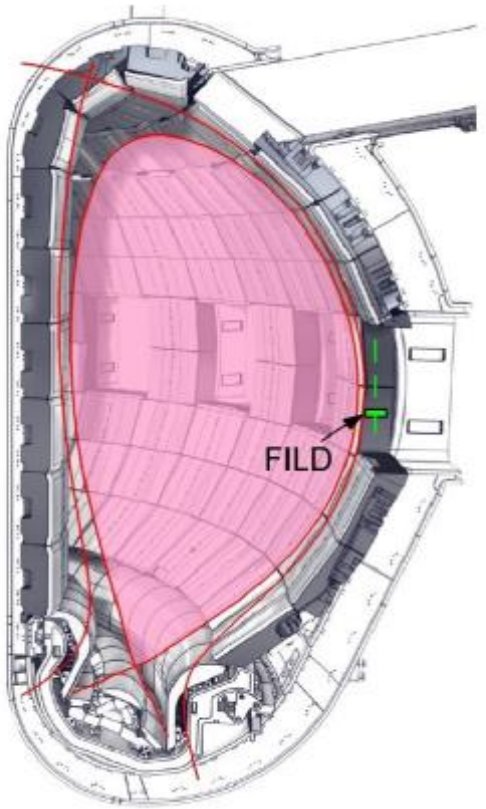

Figure 3: Poloidal cross-section of ITER

Understanding the mechanisms of losses and developing procedures for their control is one of the main avenues of research in the field of fusion. An ideal Fast-Ion Loss Detector should be able to provide information on the following aspects [9]:

- Type of suprathermic particles that are escaping from the plasma.
- Spatial location of the losses on the first wall of the reactor.
- Information about the angular distribution of the fast ions that provides information on the nature of the orbits followed by the ions.
- Good resolution in energy to detect the energy range of the suprathermic particles.
- Temporary resolution to follow the evolution and frequency of losses due to the presence of instabilities.
- The absolute flow of particles that impact on the vessel.
- The detector must be flexible and resistant to be able to withstand the harsh conditions of the hostile

environment of the fusion reactors in which it must operate.

1.3 Objectives and project scope

ITER is an experimental nuclear fusion reactor where the aim is to achieve a technology that provides clean, safe and unlimited energy. To reach this point it is necessary to study the plasma and the physical phenomena that occur during the reaction, to finally be able to control the plasma and generate energy. Hence the experimental character of the reactor.

Diagnostic systems such as FILD play an important role in understanding the process. But the fact of being incorporated in this system means that it is exposed to certain loads, such as those generated by electromagnetic disruptions.

The main objective of this master thesis is to achieve a design of FILD that is capable of resisting static loads due to electromagnetic disruptions, starting from an initial concept of device.

Other secondary objectives, but necessary to reach the main objective are:

- The general understanding of the performance of the tokamak and its components. This allowed to acquire ease for the calculation of the loads.
- Study the operation of FILD and its components to understand the conceptual design and be able to approach the design process in a realistic way.
- Learn about the different types of loads that occur in tokamaks and how they are transferred to different devices.
- Generate a valid model for the calculation of electromagnetic loads for FILD.
- Perform a finite element model to study the behavior of FILD against previously calculated loads.

1.4 Document structure

This document is composed of 5 chapters through which the objectives of the project will be completed. The following is a summary of the contents of the chapters:

- Chapter 2. FILD components. In this chapter, the main components of the tokamak are explained in order to locate FILD. In addition, the different parts of this device are described in detail in its conceptual design, as well as its operation.
- Chapter 3. Electromagnetic loads in FILD. The objective of this chapter is to obtain the value of the loads that act on FILD during an electromagnetic disruption. To do so, first the types of loads in tokamaks are exposed, to later detail the electromagnetic ones, exposing calculation examples and finally establishing a valid model to calculate the loads on FILD.
- Chapter 4. Structural analysis of FILD. The results of the analyses with the loads obtained in chapter 3 carried out are exposed. This chapter details how the analyses have been carried out, as well as the design process followed to arrive at an optimal solution that solves the static problem by modifying as little as possible the conceptual design.
- Chapter 5. Conclusions. It is dedicated to extract the conclusions of the results obtained in chapter 4 and indicate the possible future lines in which to develop new work.

2 FILD COMPONENTS

2.1 Introduction

In this section, it is intended to show the conceptual design of FILD, with a detailed description of all its parts, as well as its operation and location. Before going into detail with FILD components, it is necessary to know the internal structure of the tokamak. In the figure 4, the main components of the ITER reactor are shown.

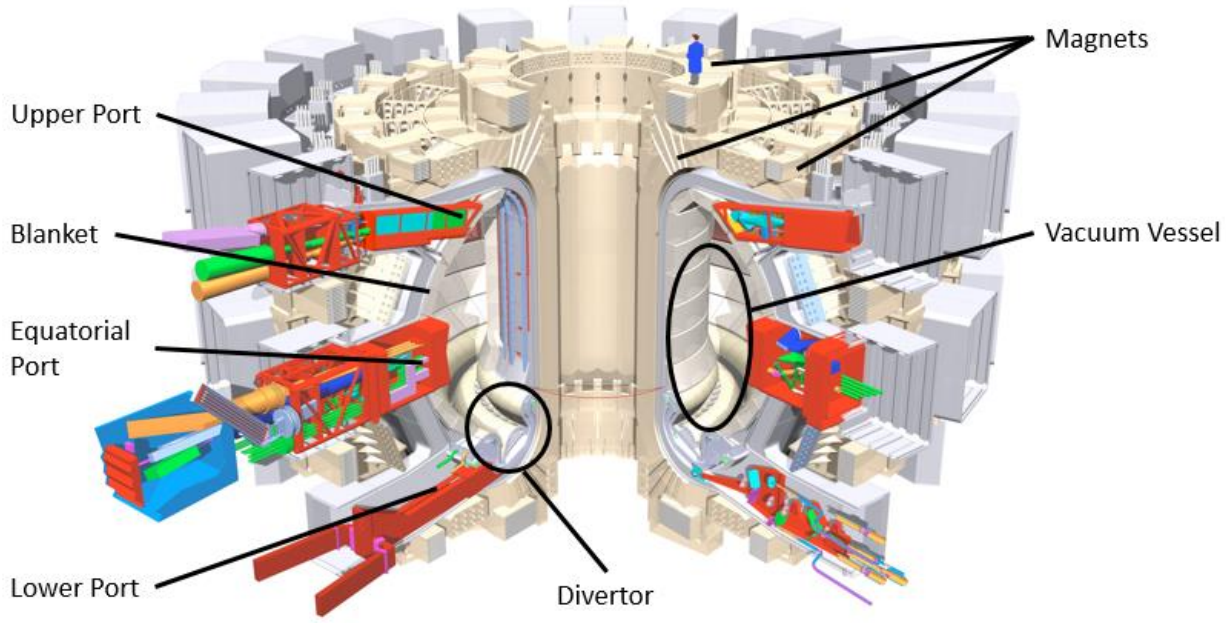

Figure 4. ITER tokamak internal structure

The main component is the Vacuum Vessel (VV). The ITER experiments will take place inside the Vacuum Vessel, a hermetically sealed steel container that houses the fusion reactions and acts as a first safety containment barrier. In its doughnut-shaped chamber, or torus, the plasma particles spiral around continuously without touching the walls [10].

Ten thousand tonnes of magnets, with a combined stored magnetic energy of 51 Gigajoules (GJ), will produce the magnetic fields that will initiate, confine, shape and control the ITER plasma. Manufactured from niobium-tin (Nb3Sn) or niobium-titanium (Nb-Ti), the magnets become superconducting when cooled with supercritical helium in the range of 4 Kelvin (-269 °C) [11].

The Vacuum Vessel provides a high-vacuum environment for the plasma, improves radiation shielding and plasma stability, acts as the primary confinement barrier for radioactivity, and provides support for in-vessel components such as the blanket and the divertor. Cooling water circulating through the vessel's double steel walls will remove the heat generated during operation.

The blanket modules that cover the inner walls of the VV protect the steel structure and the superconducting toroidal field magnets from the heat and high-energy neutrons produced by the fusion reactions [12].

Situated at the bottom of the Vacuum Vessel, the divertor extracts heat and ash produced by the fusion reaction, minimizes plasma contamination, and protects the surrounding walls from thermal and neutronic loads [13].

Forty-four openings, or ports, in the Vacuum Vessel provide access for remote handling operations, diagnostics, heating, and vacuum systems.

These openings are divided according to their location in Upper Port, Equatorial Port and Lower Port.

2.2 Location

As explained previously, FILD intends to make measurements of fast ion losses at the plasma edge, so it must be placed in a situation that can perform this type of measurements. That is why FILD is integrated in an Equatorial Port Plug #08 (EPP#08). The Equatorial Port Plugs are the central structures (Figure 5) where various diagnostic systems are located such as FILD and consists of three basic parts [14]:

- The diagnostic first walls (DFW) which serves as plasma facing parts of the assembly while developing the role of first neutron shielding layer and implements the necessary cutouts and apertures to the plasma required for the operation of diagnostic systems assembled in the PP.
- The diagnostics shielding modules (DSM), which provide the neutron shielding to port aperture in order to minimize the activation and the dose in the Port Cell (interspace) area and ports and house diagnostic and service systems.
- The EPP#08 structure as main structural element that holds the rest of components, that forms the connection to the VV being part of the primary vacuum and confinement boundaries and that provides the interface (closure plate) for all required penetrations and feedthroughs between the in-VV space and the Port Cell.

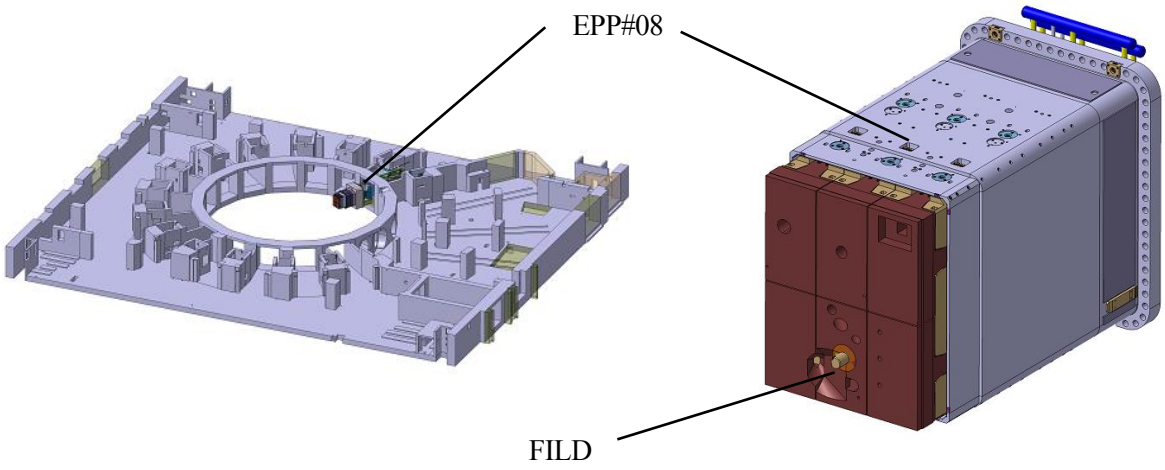

a) EPP's distribution b) FILD's location in EPP#08

Figure 5. FILD's location

The device will be installed at the EPP#08, approximately 10 cm above the midplane, oriented horizontally along the major radius of the machine [15].

The design of FILD, at conceptual design phase, is shown in figure 6, where EPP#08, DSM2 and DFW are also schematically represented. As can be seen in the figure, FILD is attached to the last vertical blade of the DSM2 by the fixed part. This fixed part serves as a support and guide for the movable part, which holds the probe head and pushes it close to the plasma for measuring.

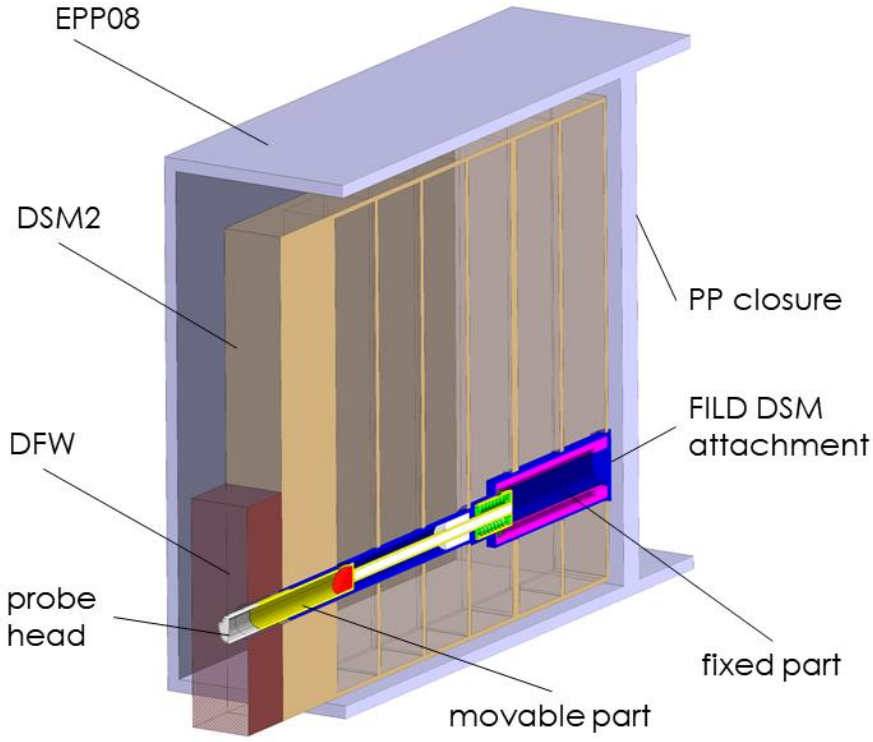

Figure 6. General scheme of FILD

2.3 General description

FILD is integrated into an EPP, but it is necessary to measure at the edge of the plasma to capture the fast ions. This fact presents a great disadvantage: The exposure to large thermal loads, which significantly limits the duration of the measurement. FILD is designed to operate in a fixed position during plasma discharge. The insertion length is previously defined and when the discharge is finished, the system automatically retracts.

To protect both the integrity of the tokamak and FILD, there is a security protocol that allows the discharge to be aborted if the measured thermal loads exceed a limit. By providing the detector with feedback for temperature control (or other measure of thermal load) it can automatically be retracted if necessary, e. g. if the thermal loads suddenly increase due to plasma displacements. Given the time scale associated with thermal variations near the plasma, rapid displacements will be required in a short period of time, to send the FILD body to a safe position. Thus, the system will have a measurement position and a parking position (Figure 7).

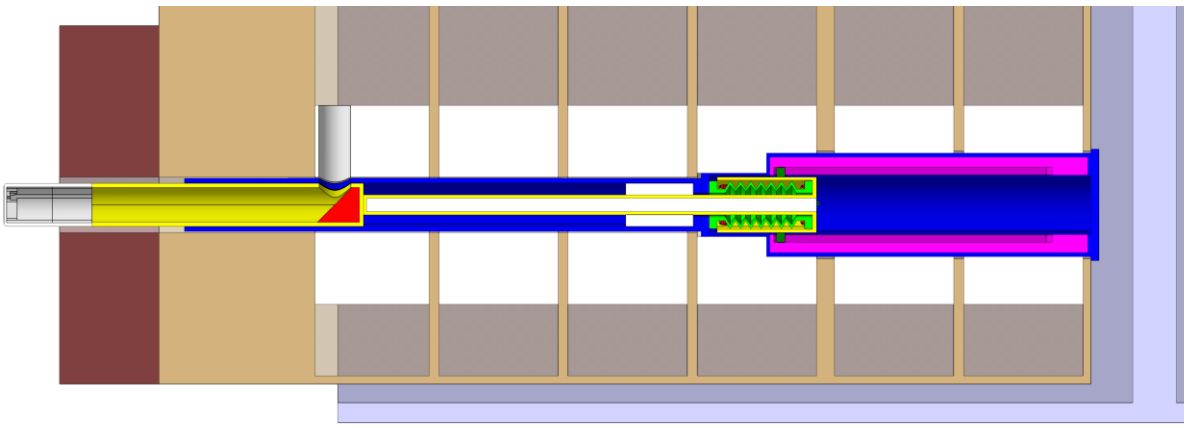

a) Measurement position

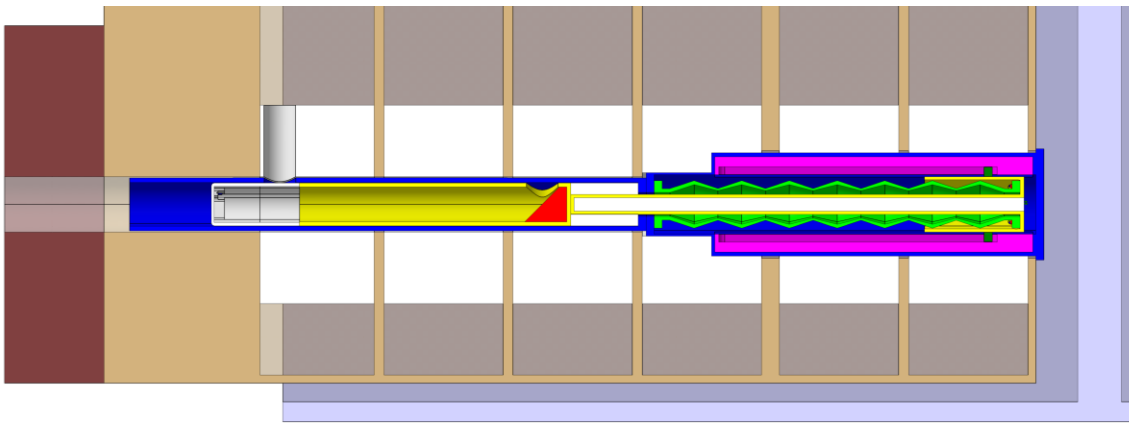

b) Parking position

Figure 7. FILD positions

In general, the different components of the diagnostic device can be summarized in:

- **Linear manipulator.** It is divided in four parts:
  - **Linear actuators.** They generate the movement in a straight line to bring the probe head closer to the plasma for measuring and to move back to the parking position.
  - **Fixed part.** Comprises the fixed support, the outer pipe (to limit the deformation of the movable part during electromagnetics transient events and/or seismic events) and the outer neutron shielding cylinder.
  - **Movable part.** Comprises the probe head, the probe head support, the guide assembly (rolling guide and rollers), the inner neutron shielding cylinder and the first mirror.
  - **The edge welded metallic bellow.** It is needed to provide a private gas chamber inside the fixed support avoiding gas leakage into de Vacuum Vessel. The bellow accommodates the reciprocating displacement of the probe avoiding in vacuum contacts between moving parts (rollers and fixed support).
- **The optical system**, consisting on several mirrors (including the optical hinge) responsible of transmitting the detector optical signal out of the port plug, back to the optical acquisition systems (camera and photomultipliers).
- Other FILD **common services** such as gas feedthrough, cabling, and electric isolating, etc.

The material of the fixed part and the movable part (except the probe head) is stainless steel 316L(N) – IG (ITER Grade).

In figure 8, the general scheme of FILD is shown with the different parts previously commented.

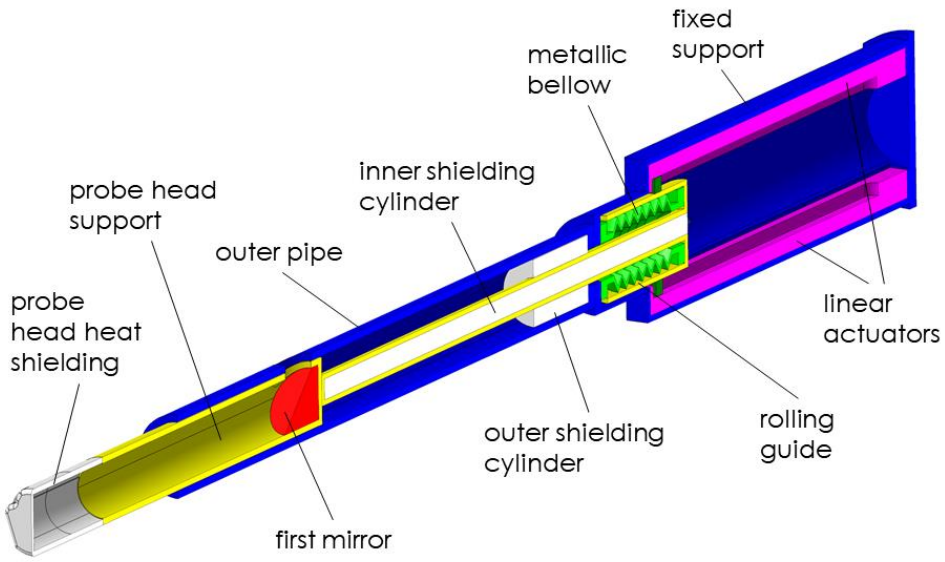

Figure 8. Main components of FILD

2.4 Probe head

Before explaining the various components of the system, it is necessary to know what the objective of FILD is. The ions that manage to escape from the plasma have a helical trajectory and must be inserted through the pinhole of the probe head.

The diagnostic probe head design consists of three basic components: scintillator plate, collimator and graphite cap, shown in figure 9. In addition, to resist the high temperature, the probe head is made of TiZnMo alloy. The collimator narrows a measurable beam from the fast-ion flux reaching the pinhole. In turn, the scintillator plate emits light when this fast-ion beam collides with it. The graphite cap serves as thermal protection to all the probe head components. The size and the relative position of these three main components determine the diagnostic resolution, intensity and measurable range [7].

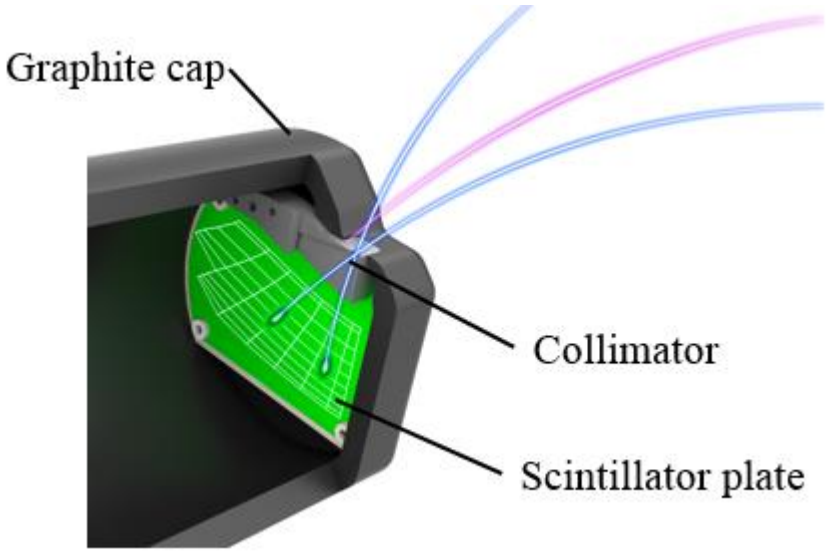

Figure 9. Schematic of FILD principle

2.5 Linear actuators

As explained previously, there are two linear actuators (Figure 8 – pink), whose main mission is to generate the linear movement of the movable part to place the probe head in the right place for measurements. Linear actuators are redundant for safety reasons.

But there is another function as important as the first, to retract the system in case of thermal overloads during electromagnetic disruptions events (release of plasma energy that can cause surface melting of plasma-oriented components [16]).

This energy discharge is very fast so electro-mechanical linear actuators that can reach a high retraction speed in a short time are required. Therefore, the Parker XE actuator has been selected (Figure 10) with the main characteristic shown in Table 1.

Figure 10. Linear actuators

Table 1. Characteristics of linear actuators

Profile width (mm)	Drive type	Maximum stroke (mm)	Maximum speed (m/s)	Maximum acceleration (m/s^2)
60,5	Ballscrew	655	0,5	20

2.6 Fixed part

The fixed part (Figure 8 – blue) is characterized by fulfilling three important functions:

- Anchoring a structure that supports the system to the last vertical blade of the EPP.
- It serves as support for linear actuators.
- Protects the movable part from excessive deformation, especially during electromagnetic disruptions and seismic events.

In addition, it acts as an enclosure where gas is introduced into the movable parts to avoid vacuum contact; as well as housing the outer neutron shielding cylinder.

2.7 Movable part

The main element of this part is the probe head, already explained previously (section 2.4.).

Movable part also contains the support of the probe head (Figure 8 – yellow), which consist of a structural element that joins the head of FILD with the linear actuators, by means of guides and rollers. This element is especially sensitive to mechanical loads, since its dimension are limited as it is inside a fixed part. The zone of the support of the probe head between the first mirror and the rollers, is a pipe filled with internal neutron shielding.

At the end of the FILD head support, there is the first mirror (Figure 8 – red), a mirror that reflects the signal emitted by de scintillator plate to send it out of the port plug through an optical system.

Finally, it is worth mentioning the existence of a metallic bellow (Figure 8 – green) whose function is to isolate the part where there is contact from which there is no contact, so that the necessary gas in the areas where there is contact is trapped in that volume (Figure 11) and does not enter the vacuum zone.

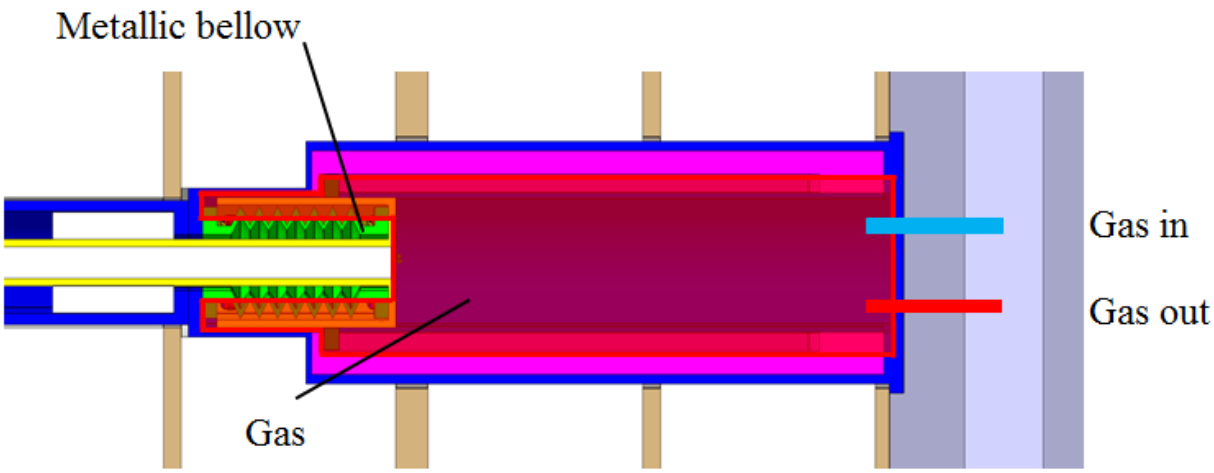

Figure 11. Gas chamber scheme

3 ELECTROMAGNETIC LOADS IN FILD

3.1 Introduction

FILD diagnostic system is subjected to a number of types of loads that shall be considered in the structural integrity evaluation of its components. They can be categorized as [17]:

- **Inertial loads due to dead weight (DW):** The dead weight of the system.
- **Plasma disruptions electromagnetic loads:** The actions derived from the electromagnetic transients constitute the dominant loads on the assembled Equatorial Port Plug and on-board components. They can be summarized in Major Disruption (MD) and Vertical Displacement Events (VDEs).
- **Inertial loads due to seismic events:** Seismic load excitation corresponds to the specific selected site (Cadarache) for the ITER construction. The ground acceleration can be both in the horizontal and in the vertical direction and typically has a spectra content which lead to some level of support reaction load amplification.
- **Thermal-hydraulic loads:** Thermal expansion stresses associated with normal full power plasma operation and with vacuum baking.
- **Nuclear loads:** Nuclear heating, damage and component activation of the Fast-Ion Loss Detector system parts and supporting structures.
- **Interface loads:** They correspond to loads transmitted through the surrounding structures like vibrations and the relative displacements between anchorage points of the different components.
- **Incident and accident loads:** Correspond to accidental events during the operation of the machine like the Loose of Coolant Accident (LOCA), pipe breaks and leakages from the blanket, divertor or other in-vessel components identified as Ingress of Coolant Event (ICE). They are treated independently.

3.2 Electromagnetic loads due to electromagnetic transients

Electromagnetic loads will occur in ITER due to transient events. These loads will be significant in the case of the diagnostic systems placed inside the port extensions or port plugs and need to be taken into account.

The specification of loads in diagnostic systems inside assembled ports caused by electromagnetic events may be divided into several parts [18]:

- **Volumetric loads from induced currents in passive structures:** The first contribution is the volumetric loads distributed in passive conducting structures. One of the main effects of the electromagnetic transient events is the induction of currents in the conducting structures which, in the presence of electromagnetic fields (Poloidal Field, PF; Toroidal Field, TF; Central Solenoid, CS; … coils) can lead to significant internal loads. In general, the transient electromagnetic event will induce two types of currents:
    - **Eddy currents**, induced by the mechanism of conservation of the magnetic fluxes (from all sources) crossing conductive parts. They are closed in loops which are fit in either a single conductive part or in a set of several interconnected conductive parts.
    - **Halo currents**, induced by the mechanism of conservation of the toroidal magnetic flux in plasma core region. The halo currents intercept the plasma facing components of the first wall during the development of the electromagnetic event forming close loops of currents through the Vacuum Vessel internal passive structures.
- **Dynamic amplification effects:** The development of the induced currents mentioned in the previous point occurs during the evolution of the electromagnetic event which is a short duration phenomenon.

Therefore, a rigorous treatment of these loads would require their consideration in a dynamic way to account for the inertial effects of the system. Indeed, this would be the second contribution. For the particular case of the assembled Port Plugs (but not limited to); as they are complex systems and dynamic analyses are usually cumbersome; a usual practice is to treat these loads in a static way. This requires first the identification of the peak forces developed during the transient. These peak forces are then, scaled by a dynamic amplification factor (DAF) to include the inertial effects. DAFs are normally determined using transient analysis in simplified models and their validity is subjected to the equivalence of the peak loads static and maximum dynamic responses of the system.

- **Inertial loads associated to Vacuum Vessel movements:** Port Plugs are assembled in the Vacuum Vessel by insertion in the port extensions. Port extensions are in turn, connected to the Vacuum Vessel through the port stubs leading to double cantilevered massive system. During the evolution of electromagnetic event, the Vacuum Vessel is subjected to similar effects as those described in the first point above. This means that the Vacuum Vessel will experience movements whose effect at port stub level is the development of additional inertia loads on assembled port plug systems. These actions, which constitute the third contribution, may be readily described by point response spectra defined at the port stub.
- **Interface loads:** Diagnostic systems inside EPPs are anchored to frame structures (EPP structure, DSM, DFW) which are actually deformable bodies. During the development of the transient electromagnetic events these structures will suffer deformations which can affect to the diagnostic components subjected to structural integrity evaluation in the form of relative displacements between the anchorage points. These interface loads would constitute the last contribution to consider in the specification of mechanical loads derived from electromagnetic events in diagnostic systems.

The two first contributions described above are normally determined through dedicated electromagnetic analysis of the components under study as part of the global process of structural integrity assessment.

The characterization of the Vacuum Vessel movements, inertial effects and related interface loads is obtained from a global dynamics analysis of the Tokamak including the different scenarios and particularities of the electromagnetic loads.

3.3 Volumetric loads from currents in structures

The dominant mechanical loads on FILD components arise from plasma disruptions; that is why this master thesis will focus on the study of this type of loads.

The rapidly changing magnetic fields associated with disruptions induce electrical eddy currents in the surrounding mechanical conductive structures which then interact with the background magnetic field, thus producing forces and torques. Unlike most mechanical loads, the load associated with the eddy currents is not simply specified but is instead dependent upon the details of the port plug hardware, including the DSM-DFW assembly, the port plug structure and how these components are electrically connected.

The path of electromagnetic volumetric load is shown in figure 12:

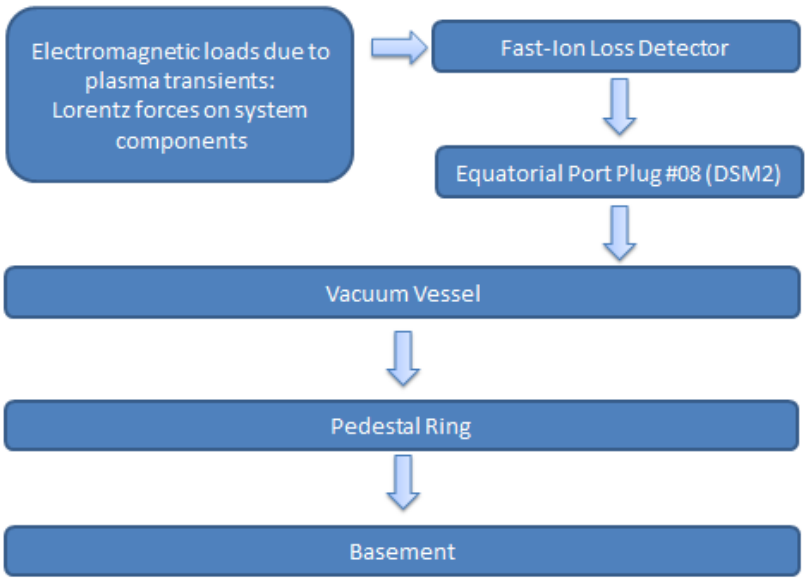

Figure 12. Path of the volumetric loads from induced currents in passive structures

Disruptions in ITER are simulated with the DINA code and the results of the DINA simulations for ITER are stored in IDM (ITER Document Management). Table 2 shows the categorization of these DINA simulations according to the ITER load specification document [19]. Additional analyses to determine worst events depending on the location are still on-going.

Table 2. ITER plasma disruptions cases and its categorization

Type of disruption	Current quench time	Peak TPF*Ihalo/Ip	Thermal quench time	Number of events
MD I	Exp. 22 ms	0,15	3 ms	2600
MD II	Exp. 16 ms	0,15	1 ms	400
MD III	Exp. 16 ms	0,15	0,5 ms	-
MD IV	Exp. 11,3 ms	0,15	0,5 ms	-
MD IVslow fast				-
VDE II slow	50 – 100 ms	0,34/0,42		150
VDE II fast	Exp. 16 ms	0,2/0,25		150
VDE III slow	> 200 ms	0,75/0,6		-
VDE III fast	Exp. 16 ms	0,36/0,45		-
VDE IV slow fast		0,6/0,75		-

Eddy currents do exist in principle (with different intensities) at any time moment of any transient electromagnetic events including normal operation, but halo current is considered only at latter phase of Vertical Displacement Events (VDEs) and Major Disruption (MDs), when the separatrix touches the plasma-facing conducting wall.

Maximum electromagnetic loads on the Port Plug components are caused by three kinds of abnormal terminations of plasma pulse:

- A MD consists of an abnormal termination of the plasma pulse consisting of two phases, the thermal quench with a fast loss of the plasma thermal energy and the current quench with a fast drop in plasma current often accompanied by a vertical drift and compression of the plasma core.
- A VDE consists of an abnormal termination of the plasma pulse initiated by a failure of vertical position control, followed by an irreversible plasma vertical drift, compression of the plasma core, the thermal quench, plasma current decay and by a further compression of the plasma core.
- A MFD (Magnet Fast Discharge) is an event where the current that flows in the ITER magnets is rapidly brought to zero (usually done intentionally after the detection of a quench to protect the coils from overheating).

In both VDEs and MDs the halo current can reach very large fractions of the total plasma current once the plasma touches the wall. In both cases the final stages include a plasma drift to either upper or lower part of the VV.

There are two types of MFD. MFD I which corresponds to a fast discharge of the CS (Central Solenoid) and PFC (Poloidal Field Coils) only, or MFD II where all coils are discharged. During a MFD I, the eddy currents created are similar to those generated during plasma initiation. During MFD II, larger loads will occur. Nevertheless, these loads are considered very small because the IVCs (in-vessel components) are not electrically connected in the toroidal and Poloidal direction. Besides, the load due to MFD is not really superimposed to the disruption loads because the current decay of MFD is much longer than the plasma disruption time.

3.4 Analysis techniques for calculation of electromagnetic loads

Below are exposed several methods used in a multitude of systems to calculate electromagnetic loads.

Procedure 1: Approach based on DINA inputs.

The general approach for calculation of EM loads is based on the EM transient analysis of the components where the eddy and halo currents are usually calculated with different kinds of inputs [14]:

- Typical input for the calculation of eddy currents caused by diamagnetic flux loss at the time of thermal quench is a current waveform in a set of poloidal loops located in plasma volume. These loops form a toroidal solenoid. The variation of the diamagnetic flux is prescribed by the DINA code. Some resultant variations of plasma shape, plasma current and the Poloidal magnetic field take place at the time of thermal quench.
- Typical input for the calculation of eddy currents caused by plasma current quench is a set of current waveforms in the toroidal coaxial loops which represent plasma evolution (time dependent net current, position, shape and current density profile). The current waveforms in these loops are provided by DINA.
- Typical input for calculation of halo currents is the time dependent poloidal profile of halo current density on the surface where the halo current intercepts the PFCs. This profile is provided by DINA.
- EM loads on the Port plug system components, as output of 3D EM transient numerical analysis, are initially represented in the form of distributed force density. These results are then transmitted further for the supporting stress-strain static and dynamic analysis of the components. The EM loads applied to each component are summarized as 6 time-dependent orthogonal components: 3 integral moments and 3 integral forces.

- Typically, EM analysis and load integration are done separately for eddy and halo current related loads, giving as output 6+6=12 time-dependent integral load components. The time dependent graphics of such integral loads indicate the peaks of each component and the time moment when each peak occurs. Note that the peaks of different load components can be reached at different times and even in different plasma events.

Electromagnetic (EM) loads (either by eddy currents or by a sum of eddy and halo) exist in each conductive part of the machine during each transient EM event. They can be represented as time-dependent 3-D vector field of force density (F=J x B), where B is time-dependent vector sum of magnetic fields by all sources at each spot and J is vector of sum current densities at each spot.

Procedure 2: Approach based on previous magnetic field solutions

An alternative approach much easier to apply in the one based on the maps of the magnetic field evolution in space envelope where components sit. The loads due to the induced currents are mostly dominated by the plasma transients and the large CS, PF and TF currents, hardly affected by the local variation in effective conductivity. Given the maps of evolution of the magnetic field in the region of interest the electromagnetic loads can be estimated using a local electromagnetic model of the assembled components in the PP including the components under study can be used. The fields provided as inputs can be interpolated in the local finite element mesh. Figure 13 shows the volumetric force density in an entire port plug [20].

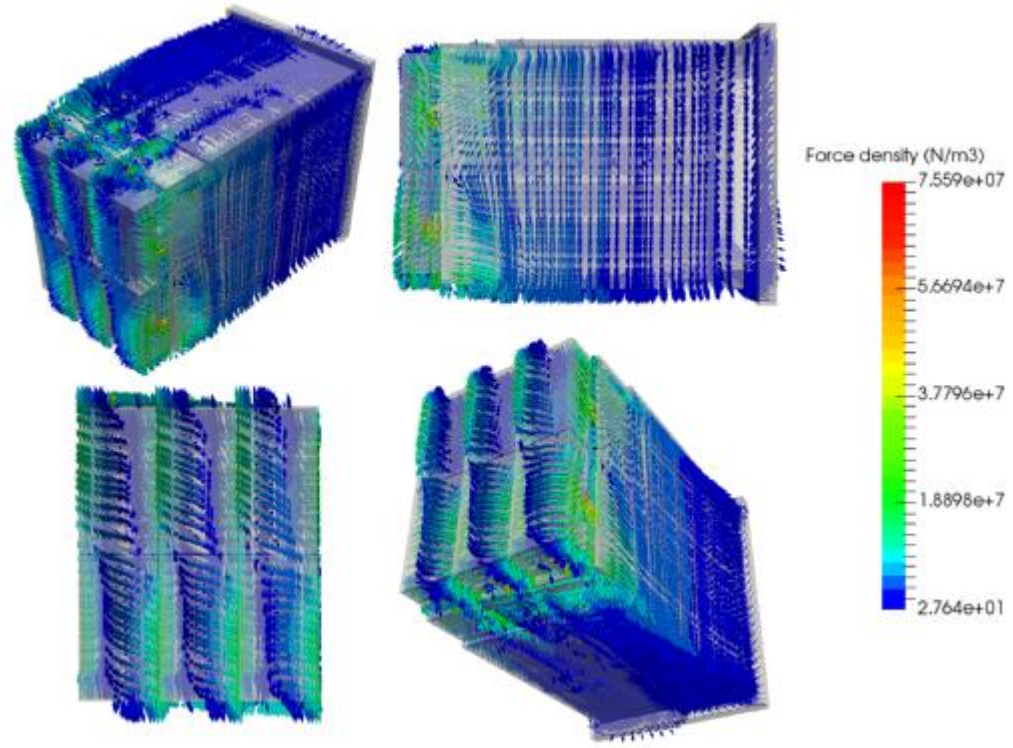

Figure 13. Force density distribution to be interpolated in the whole port plug (N/m^3)

This interpolation depends on the formulation of the electromagnetic analysis, nevertheless it would be performed as imposed boundary conditions in the whole domain simulated considering the particular degrees of freedom in consistency with the formulation chosen.

Volumetric electromagnetic forces may be the determined as a time-dependent 3-D vector field of force density (F= J x B).

However, these activities have not been performed for the Fast-Ion Loss Detector. Therefore, the electromagnetic loads presented in this master thesis have to be valid estimates for the conceptual design review. The following sections show this estimate, starting with the definition of the geometry and later the calculation

models based on the Lorentz law.

On the sensors, eddy currents will be induced as a result of the induced voltages in the structures because of the variation of the fields during the transient events. As a result, torques will appear. In addition to that, a shared current with the supporting structure (DSM) will produce net forces on the in-port cameras.

3.5 FILD geometry for electromagnetic analysis

The geometry under study consists of the probe head, the support of the probe head and the support of the rollers; that is to say the movable part. The fixed part will only be taken into account in case there are large deformations, so it is necessary to study the interaction between the fixed and movable part.

To facilitate the calculation of electromagnetic loads, as well as finite element analysis; a simplified CAD model has been used. In this model, unnecessary elements such as the detailed shape of the probe head have been eliminated or rounding has been added in the foreseeable tension concentrator.

Figure 14-a shows an overview of the CAD model of FILD, and figure 14-b shows a cross section of the movable part under study.

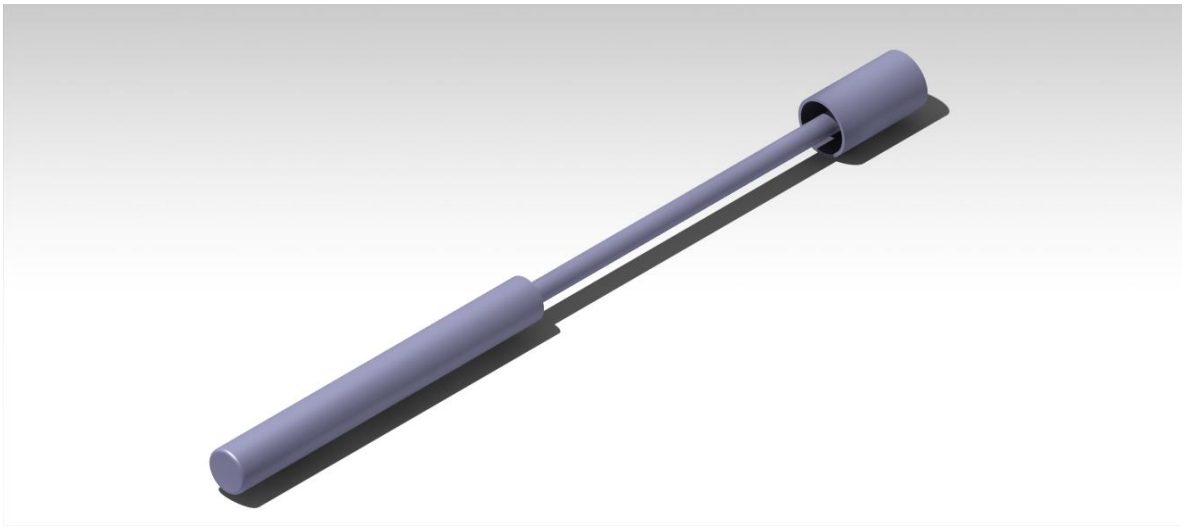

a) FILD CAD model general view

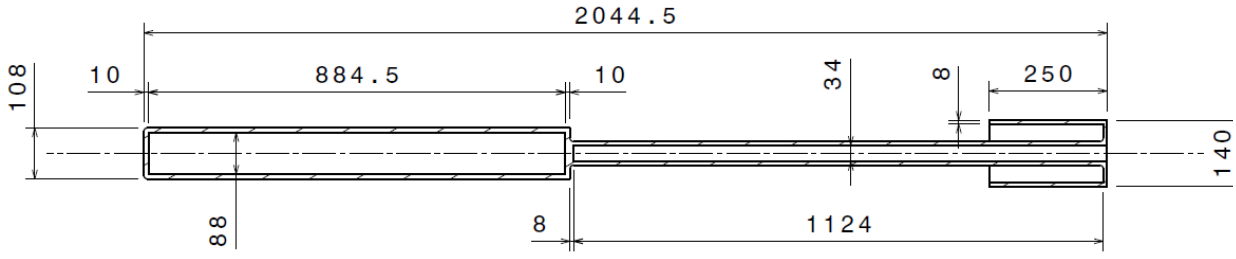

b) Cross section in the medium plane. The dimensions are shown un millimeters. All roundings have radius of 7,5 mm.

Figure 14. FILD CAD model

3.6 Estimation of electromagnetic loads

Once the geometry to be studied is defined, it is intended to calculate the electromagnetic loads that must be supported by FILD during a disruption event. As explained above, detailed electromagnetic analyses of disruptions over FILD and EPP # 08 have not been performed yet. Therefore, electromagnetic loads must be estimated from values obtained from analyses carried out in other zones of ITER or in other diagnostic systems.

The main objective of these estimations is to verify the structural integrity of FILD in a first study against electromagnetic disruptions, and thus be able to validate or make the opportune changes in the conceptual design in front of this type of loads.

The first step for estimating is to create a physical model of the problem, on which applying the various physical laws is simple.

Later, translating that model to the FILD geometry, decomposing it in several parts to facilitate the calculation.

The next step is to obtain the current that circulates through FILD, which can be of two types:

- Eddy current induced by the mechanism of conservation of the magnetic fluxes crossing the electrically conducting parts. They are closed current loops that being inside a magnetic field causes torques to appear on FILD by the Lorentz law (which acts like a loop).
- Halo currents flow in loop formed partly by conducting structures and partly by the plasma scrape-off layer. This current inside a magnetic field causes forces in FILD by the Lorentz law (which acts like a conductor).

The last step is to calculate these loads which are the beginning of the mechanical problem.

3.6.1 Eddy currents

The eddy currents tend to dominate in the thermal quench phase, at the beginning of disruption event and their time scale is small. The electromagnetic loads due to eddy currents can be calculated considering:

- The magnetic field components and their variation in time in region in which they are located.
- The current induced estimated by assuming a conductor loop with all the material lumped around the perimeter loop.

The area of the flux can be considered as the area facing the variation of the field.

Because there is no magnetic field variation data in Equatorial Port Plug #08, these values are approximated by taking them from another region similar to where FILD is located. Specifically, there are electromagnetic analysis results in the Equatorial Port Plug #01 that provide an estimate of the magnetic field variation, as well as the value of the static toroidal magnetic field (Table 3).

Table 3. Estimation of static toroidal field B_t and the variation of electromagnetic field in EPP #01

Equatorial Port #01 Cameras		
Variation of radial field dB_x/dt (T/s)	Variation of vertical field dB_z/dt (T/s)	Static toroidal field B_t (T)
11,1	70,9	5,6

The values provided in the previous table are enveloping all the electromagnetic events, as the maximum static and variation of field has been taken in each case. This is a very conservative assumption, as the maximum static field and field variation values can happen in different disruption events or time instant.

As can be seen in table 3, there are magnetic field variation values in both the radial and vertical directions. This generates that current is induced in two different directions, and therefore there are torques in two directions

which are calculated independently.

3.6.1.1 Eddy current due to variation of radial field

The model used to calculate the eddy currents due to the variation of the radial field is an open tube whose longitudinal direction is parallel to the field variation (which is known). That is why, according to Faraday's law, the induced electromotive force in any closed circuit is equal to the negative of the time rate of change of the magnetic flux enclosed by the circuit.

To carry out the calculations, cylindrical differential elements (dr) of radius r and length L will be taken as shown in the figure 15.

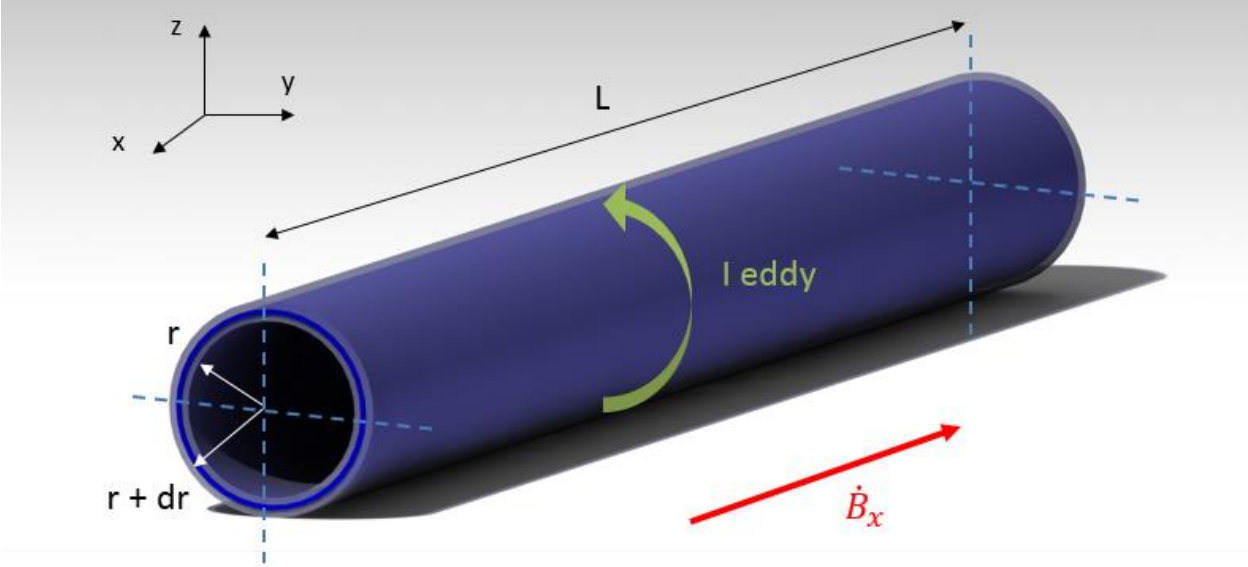

Figure 15. Model for electromagnetic calculations (radial field variation)

Radial field variation induces an electromotive force, and by symmetry the induced currents (I eddy; figure 15) will have the shape of circles centered on the axis of the cylinder.

The flow (Φ) through one of these cylindrical elements is the magnetic field multiplied by the area that faces the magnetic flux variation.

$$\Phi = B \cdot \pi \cdot r^2$$

The electromotive force induced (ε) in the element of radius r is:

$$\varepsilon = -\frac{d\Phi}{dt} = -\pi \cdot r^2 \cdot \dot{B}_x$$

As can be seen from the previous equation the induced electromotive force (emf) is variable depending on the radius. The negative sign of ε means that the direction of the induced current is such that it opposes the flow variation, therefore, the direction of the induced current is shown in figure 15 and the negative sign will be eliminated in the next expressions. This emf is the one that sets in motion the charge carriers contained in the cylindrical layer volume of length L between r and r + dr, originating a current:

$$di = \frac{\varepsilon}{dR_e}$$

being dR_e the resistance of a tube of length $2 \cdot \pi \cdot r$ and section $L \cdot dr$, through which the current flows. The resistance is:

$$dR_e = \rho \frac{2 \cdot \pi \cdot r}{L \cdot dr}$$

where ρ is the resistivity of the material.

The current flowing in the differential section is:

$$di = \frac{\pi \cdot r^2 \cdot \dot{B}_x \cdot L \cdot dr}{2 \cdot \rho \cdot \pi \cdot r} = \frac{\dot{B}_x \cdot L \cdot r \cdot dr}{2 \cdot \rho}$$

Once obtained the differential expression of the intensity, the next step is to integrate it between the major and minor radius (b and a, respectively) to calculate the total intensity that circulates through the tube.

$$I = \int_a^b \frac{\dot{B}_x \cdot L \cdot r}{2 \cdot \rho} dr = \frac{\dot{B}_x \cdot L}{4 \cdot \rho} \cdot [b^2 - a^2]$$

With the calculation of the induced intensity, the proposed model is solved, so it will be necessary to transfer the model to FILD geometry. Comparing figures 14 and 15, it is concluded that FILD con be modeled as two cylinders of different dimensions in which two intensities will circulate.

First, the intensity (I_1) that flows through the larger cylinder (radius 54 and 44 mm) is calculated:

$$I_1 = 3324\ A$$

On the other hand, the intensity that circulates through the smaller cylinder (radius 25 and 17 mm) is:

$$I_2 = 1437\ A$$

These intensities that circulate through FILD as if it were a loop, are immersed in a toroidal static magnetic field, so by the Lorentz law there are moments. The moment can be expressed as a vector product of two vectors, the magnetic moment vector $\vec{m}$ and the magnetic field vector $\vec{B}$.

The modulus of the magnetic moment vector is the product of the intensity by the area of the loop (it is considered the largest area to be conservative, and all the material in a single loop). Its direction is perpendicular to the plane of the loop and it is determined by the progress of a corkscrew that rotates as the current does in the loop. The magnetic field vector is the static toroidal field which is shown in figure 16.

Performing the vector product described above, the following expression is obtained to calculate the moment:

$$M = S \cdot I \cdot B_t$$

being S, the surface of the loop (largest surface); I, the intensity previously calculated; and B_t, the static magnetic field.

Particularizing for the two intensities, the moments M_1 and M_2 result with the directions shown in figure 16.

$$M_1 = 171\ N \cdot m$$

$$M_2 = 16\ N \cdot m$$

The resulting moments are bending moments in the z-axis applied to the principle of the major and minor cylinders.

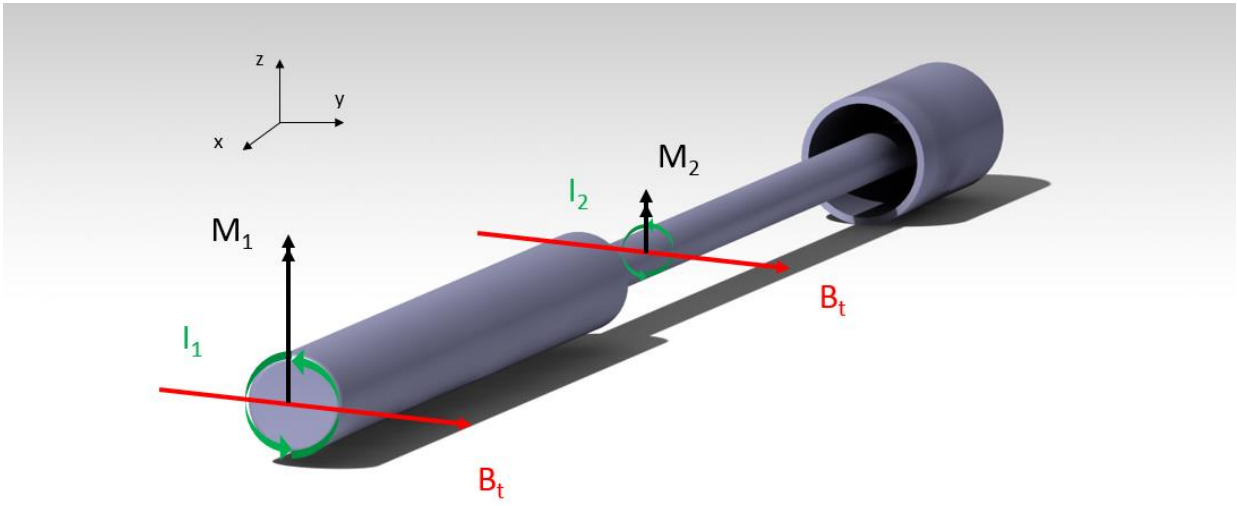

Figure 16. Moments in z-axis due to eddy currents

3.6.1.2 Eddy current due to variation of vertical field

The model used to calculate the eddy currents due to the variation of the vertical field is a closed tube (to close the circuit) whose longitudinal direction is perpendicular to the field variation (which is known).

In this case, to perform the calculations, sheets have been taken along the z-axis of thickness dz. The length of the cylinder is L. The width of the sheet in x direction depends on the distance z of the sheet and is $2 \cdot \sqrt{R^2 - z^2}$. Finally, the thickness in the y direction is δ.

The model is shown in the figure 17:

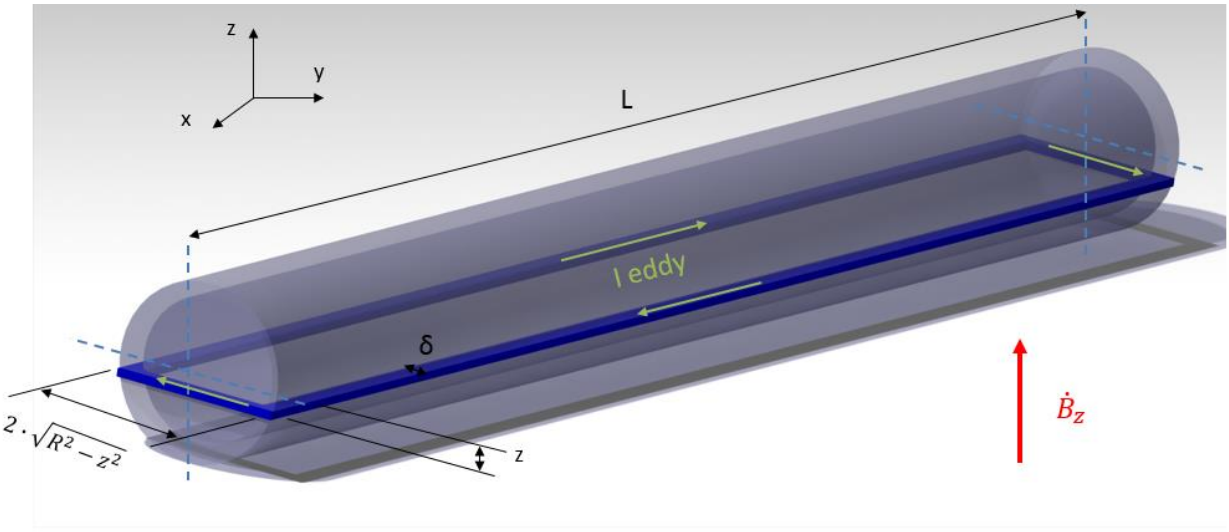

Figure 17. Model for electromagnetic calculations (vertical field variation)

The magnetic flux defined by the magnetic field multiplied by the area facing the variation of magnetic field:

$$\Phi = B \cdot 2 \cdot \sqrt{R^2 - z^2} \cdot L$$

By performing the same procedure as in the previous case, the induced electromotive force is calculated:

$$\varepsilon = -\frac{d\Phi}{dt} = -\dot{B}_z \cdot 2 \cdot \sqrt{R^2 - z^2} \cdot L$$

The induced electromotive force is opposed to the effect of magnetic flux variation hence the negative sign and direction of induced intensity (I eddy) shown in figure 17.

The resistance of each of the sheets of dr is calculated taking into account a length of $(4 \cdot \sqrt{R^2 - z^2} + 2 \cdot L)$ and a section of $\delta \cdot dz$.

$$dRe = \rho \cdot \frac{(4 \cdot \sqrt{R^2 - z^2} + 2 \cdot L)}{\delta \cdot \mathrm{dz}}$$

The intensity in one of the differential loops is the emf divided by the electrical resistance:

$$di = \frac{\dot{B}_z \cdot 2 \cdot \sqrt{R^2 - z^2} \cdot L \cdot \delta}{\rho \cdot (4 \cdot \sqrt{R^2 - z^2} + 2 \cdot L)} \cdot \mathrm{dz}$$

To obtain the intensity that circulates through the tube it is necessary to integrate all the sheets between -R and R (along the z-axis):

$$I = \int_{-R}^{R} \frac{\dot{B}_z \cdot 2 \cdot \sqrt{R^2 - z^2} \cdot L \cdot \delta}{\rho \cdot (4 \cdot \sqrt{R^2 - z^2} + 2 \cdot L)} \cdot \mathrm{dz}$$

Due to the complexity of solving this integral analytically, a numerical calculation software has been used to solve it. Therefore, the model has been transferred directly to FILD dimensions in the same way as in the previous section.

An intensity has been calculated for the outer diameter tube 54 mm (I_1) and another for the 25 mm diameter (I_2):

$$I_1 = 3987\ A$$

$$I_2 = 726\ A$$

In the same way as previously, the torques that generate the induced intensities on FILD are calculated. Again, two separate loops are considered so that two torques will be obtained, in this case of torsion (Figure 18)

$$M_1 = 2181\ N \cdot m$$

$$M_2 = 232\ N \cdot m$$

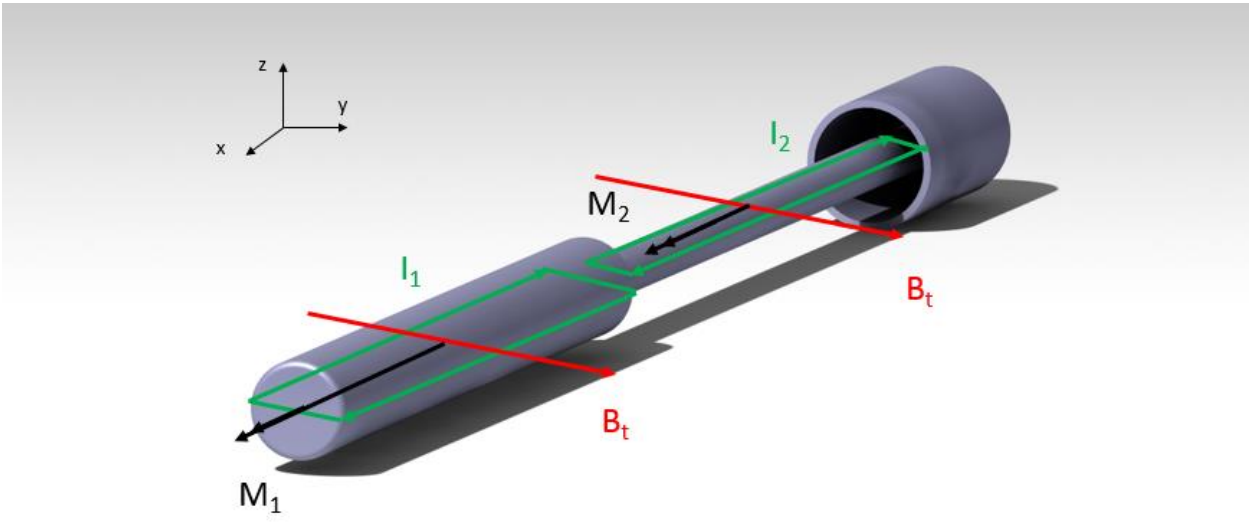

Figure 18. Moments in x-axis due to eddy currents

From these results it can be concluded that the greatest load is produced by torsion, which is corroborated by other studies [21]. There is also some flexion in the z-axis that is less important than torsion. As a summary, loads by eddy currents are shown in table 4.

Table 4. Eddy current loads

Larger cylinder		Smaller cylinder	
Torsion ($N \cdot m$)	Flexion ($N \cdot m$)	Torsion ($N \cdot m$)	Flexion ($N \cdot m$)
2181	171	232	16

3.6.2 Halo currents

Detailed examinations of electromagnetic and heat loads under various disruption conditions expected in ITER are essential to check the robustness of the design against the potential consequential loads. Robustness of the Vacuum Vessel and large in-vessel components, such as the blanket modules and divertor cassette, are particularly important since they are directly linked with the protection of the machine against mechanical damage. Robustness of the heat load during the thermal quench and vertical displacement events, which may cause possible damage to the plasma facing components, is another important point.

Due to the measurement of fast ions carried out by FILD, it is required that it be close to the plasma, which makes it a candidate to support electromagnetic loads by halo current circulation during a disruption.

Halo currents are electrical currents that flow from the charged and hot plasma that feeds the fusion reactions and hits the walls of the fusion facilities. The main difference with eddy currents is that it is not an induced current, otherwise the plasma current itself flows through the elements. They also occur during disruption events but only in the last phase.

There are simulations [22] that show that vertical displacement events (VDEs) and Major Disruptions (MD) in ITER can generate a few MA Halo currents. Figure 19 shows time evolutions of the plasma current (red), the vertical position (blue) and the poloidal halo current (green) for an upward and downward VDE. In addition, it is concluded that when there is a faster current quench, lower halo current appears (Figure 19 – a fast, b slow).

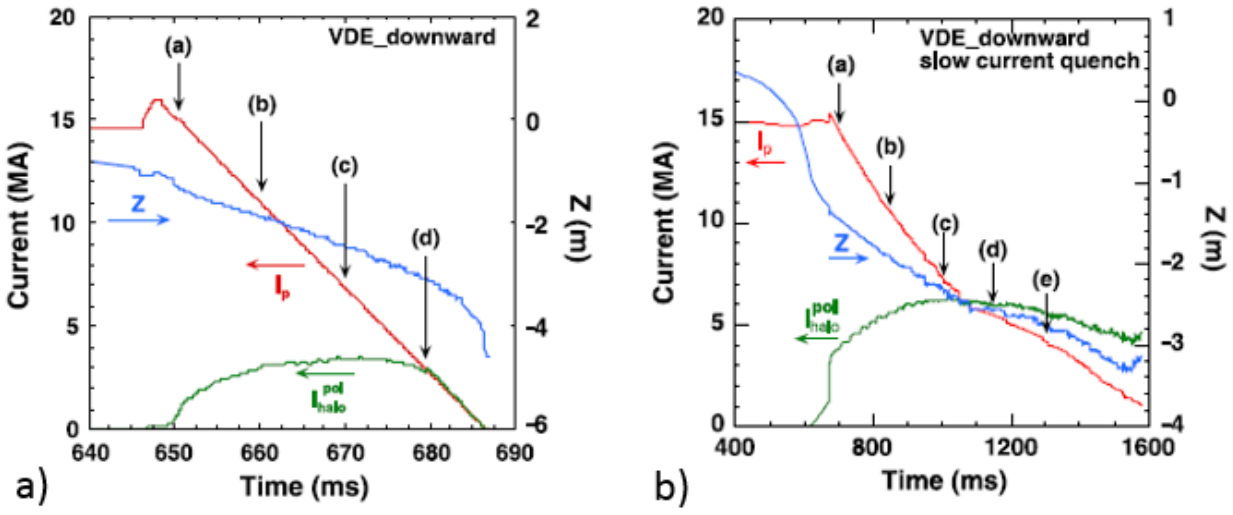

Figure 19. Time evolutions of the plasma current, vertical position and poloidal halo current.

a) VDE downward. b) VDE downward slow current quench

In this study, the calculation of halo current is based on the document ITER Load Specification [19]. VDE II and MD I cases have been considered the most damaging to be on the security side. VDE III has not been considered as it happens only a few times in the ITER life. It is also assumed conservatively that Halo currents will flow through the FILD to DSM rather than returning to plasma.

The existence of Halo currents in Equatorial Port is a discussed topic, since from the DINA simulations, it is extracted that the Halo boundary are far away. That is why I_{halo} calculated below represent an engineering assumption, there are not specific DINA simulation associated to it. Considering the existence of Halo current in EP the calculations are on the security side since the I_{halo} to EP would be overshoot of the plasma position control e.g. error in the control of the plasma-wall outer gap but the response for this error takes a few seconds.

VDE II case:

The steps to calculate the halo current in FILD during a VDE II are:

- From ITER Load Specification [19], it is extracted that the poloidal Halo current for VDE III to the Equatorial Port aligned with the surrounding blankets is:

$$I_{EP}\ (VDE\ III) = 103\ kA$$

- The same document states that in VDE II cases, the maximum halo current values for the in-vessel components correspond to 56% of the VDE III cases:

$$I_{EP}\ (VDE\ II) = 58\ kA$$

- Assuming conservatively, that through FILD circulates the same Halo current density as the Equatorial Port above; poloidal Halo current to the FILD can be estimated by considering the diameter of the probe head and the length at which the Halo current is distributed in the Equatorial Port [23]as shown in figure 20.

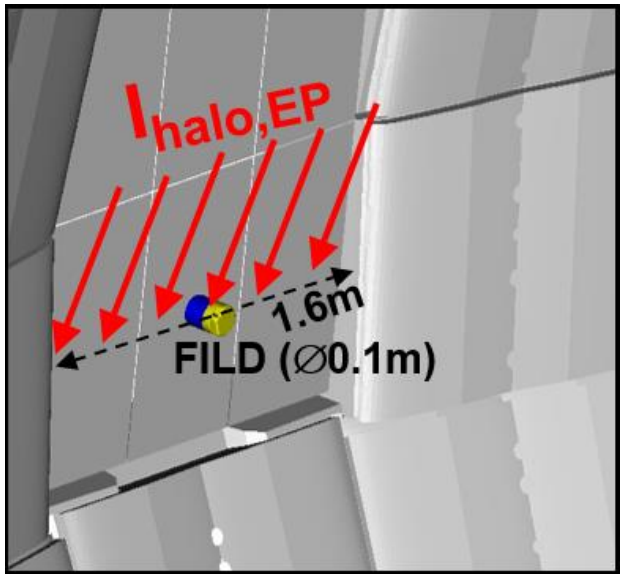

Figure 20. Halo current distributed in the toroidal width of the EPP#08

$$I_{FILD} = \frac{0{,}1}{1{,}6} \cdot I_{EP}\ (VDE\ II) = 3{,}6\ kA$$

During a slow VDE II a Halo current of 3,6 kA circulates through FILD, which is immersed in a magnetic field and a force can be generated according to the Lorentz law.

MD I case:

For the MD I case, a similar procedure is used to calculate the Halo current through FILD:

- The poloidal Halo current for MD I (fast) to the Equatorial Port aligned with the surrounding blankets is:

$$I_{EP}\ (MD\ I) = 21\ kA$$

- Halo current intercepted by inserted FILD is:

$$I_{FILD} = \frac{0{,}1}{1{,}6} \cdot I_{EP}\ (MD\ I) = 1{,}3\ kA$$

In the same way, this intensity can generate a distributed force along FILD.

Before calculating this distributed force, it is important to analyze the different possible scenarios, since it is possible that retracting FILD a distance of approximately 10 cm will prevent the existence of Halo currents.

VDEs can be detected before the thermal quench (when Halo currents occur) and will be mitigated with very high reliability. FILD will have approximately 100 ms to retract before significant Halo current is generated.

MDs can be detected at the time of the thermal quench. If they are radiation-less they will have slow current quench and would develop a substantial halo current. But there is enough time (~100 ms) to activate DSM and/or retract the FILD.

Radiative MD will have a fast-current quench and fast development of the Halo current (10 ms) but I_{halo} will be lower compared to slow current quench MD or VDE. Such fast retraction would generate larger forces than the Halo current itself.

Finally, to be as conservative as possible, the VDE II case will be studied. In this way, higher loads will be obtained and the final design will contemplate the case that the retraction system fails.

The existence of a current within a magnetic field, according to the Lorentz law particularized for a rectilinear conductor, generates a force equal to the following expression:

$$F = i \cdot \int (\overrightarrow{u_t} x \vec{B}) dl$$

Being i, the Halo current; $\overrightarrow{u_t}$ a unit vector in the direction of the intensity; $\vec{B}$, the magnetic field vector and dl the length differential.

As the terms of the integral are constant, the following expression can be obtained:

$$F = I_{Halo} \cdot B_t \cdot L$$

So, considering a static toroidal magnetic field in this case of 4T [23] and a total length of 2044,5 mm (Figure 14), the result is:

$$F = 29{,}4\ kN$$

But to perform the mechanical analysis it is more realistic to consider a distributed load, which is achieved by dividing the previous expression by the length:

$$q = I_{Halo} \cdot B_t = 14{,}4\ \frac{kN}{m}$$

In the figure 21, the distributed load and the directions of vectors are shown.

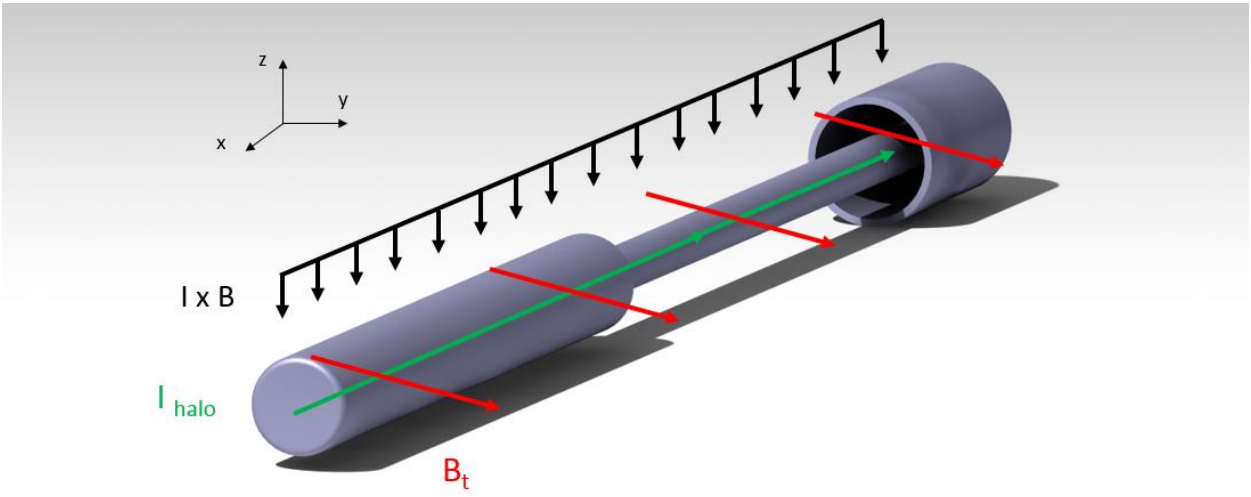

Figure 21. Distributed force due to Halo current

4 STRUCTURAL ANALYSIS OF FILD

4.1 Introduction

The objective of this chapter is to evaluate the electromagnetic loads calculated in chapter 3 (Eddy and Halo currents) to check the structural integrity of FILD during an electromagnetic disruption. Because the existence of Halo currents in this type of devices is not proven, the simultaneity of both load cases will not be taken into account.

The FILD design described in chapter 2 is a conceptual design on which there is no evaluation of loads or previous sizing, but it does take certain aspects into account.

- The available space.
- A compact design anchored in the last vertical blade of DSM.
- Hollow interior to reduce weight and accommodate the optical system.
- The balance between thermal load and alpha particle fluxes expected.
- A movable system within the fixed part.

Therefore, although the structural integrity is evaluated and changes proposed, they will always be done maintaining the conceptual idea.

The geometry under study in this chapter is the movable part described in chapter 2 and whose dimensions in detail are shown in figure 14. In case the deformations are excessive and there is no other way to support the stresses generated by the applied loads, the effect of the fixed part will be included that will help the movable part to resist.

To carry out structural integrity calculations using finite elements, ANSYS software will be used.

4.2 Material

One of the most important aspects of design is the material. The device is exposed to very adverse conditions, not only mechanical electromagnetic or seismic loads, but also electrical, magnetic due to large magnetic fields, and thermal.

The material that is capable of supporting this type of conditions is steel, but it is also required that it be stainless and non-magnetic. For this reason, austenitic stainless steel has been selected: 316L(N)-IG (ITER grade).

This is the best material for this type of components thanks to its low magnetic permeability (<1,03), the radioprotection, the controlled nitrogen content, and its mechanical properties [24].

As is done in other studies [21], for loading category III (unlikely) or category condition emergency, the $3 \cdot S_m$ rule is proposed. By this rule the occurrence of progressive deformation on the basis of elastic analysis can be prevented if the elastic peak stress is below the $3 \cdot S_m$ level of the material. For the FILD material $3 \cdot S_m = 270$ MPa. This value is corroborated in dedicates studies of this material [25]. It also has a minimum tensile strength of 525 MPa.

Its yielding strength provide very good mechanical properties; its low magnetic permeability gives it a non-magnetic behavior and its Cobalt, Niobium and Tantalum content give it the characteristic of radioprotection.

To perform the simulations, the ANSYS Stainless Steel material is taken whose properties are similar to the 316L(N)-IG.

4.3 Eddy current loads analysis

In this section the static analysis of FILD will be carried out to ensure the structural integrity against of the loads generated by eddy currents.

Then, the different aspects of the model (meshing, boundary conditions) will be discussed before commenting on the results.

4.3.1 Mesh

Meshing can be considered the most important process in the calculation with finite elements, since the results and their reliability will depend on the chosen mesh. The factors to take into account in this process are the type of element with which it will be meshed, and their distribution in the geometry.

The choice of the type of element is linked to the results wanted to extract with the analysis in question, since each of them is programmed for a specific purpose.

The distribution in the geometry refers to the use of different element sizes (mesh refinement) to take advantage of computational resources and refine the calculation in areas of interest for the obtaining results, or else, in which important stress/strain gradients are produced to guarantee their correct transmission. On the other hand, it also depends on the distribution of elements, their quality, since a uniform and orderly distribution gives rise to elements with better aspect ratio (less deformation), improving the results obtained.

Tetrahedral elements can fit better complex geometry. However, the integration of the shape functions with points of Gauss is less accurate than hexahedral elements. In addition, one of the factors that determines the quality of the mesh is the distortion of the elements.

As the geometry to be studied is not very complicated, mostly hexahedral elements (Hex20 element) have been used. The idea of meshing is to generate a regular mesh, without distortions and faithfully reproduce the geometry. For this it is necessary that the mesh can be refined a lot, but it is also possible, through sensitivity analysis, to obtain a compromise between coarse mesh (lower computational cost) and precision of calculations.

Figure 22 shows an example of fine hexahedral mesh, although throughout the evolution of the analysis a thicker mesh with similar stress results will be sought. The details of the stress concentrator are also shown, because they are areas where a high element density is necessary to capture the stress concentration effect. The mesh shown has 233100 elements.

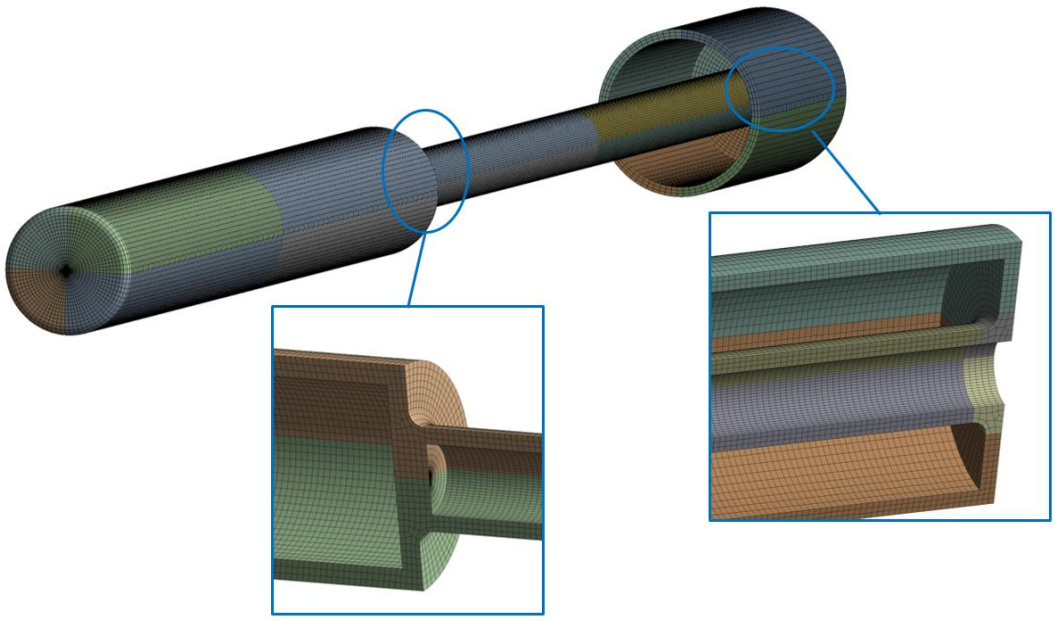

Figure 22. Mesh in eddy current model

There are two parameters that give an idea of the quality of the mesh and these are:

- Element quality: A value of 1 indicates a perfect cube or square while a value of 0 indicates that the element has a zero or negative volume.
- Aspect ratio: The aspect ratio is the ratio between its largest and smallest dimension.

Element quality (Figure 23 – a) and aspect ratio (Figure 23 – b) of the previous mesh are shown un Figure 23.

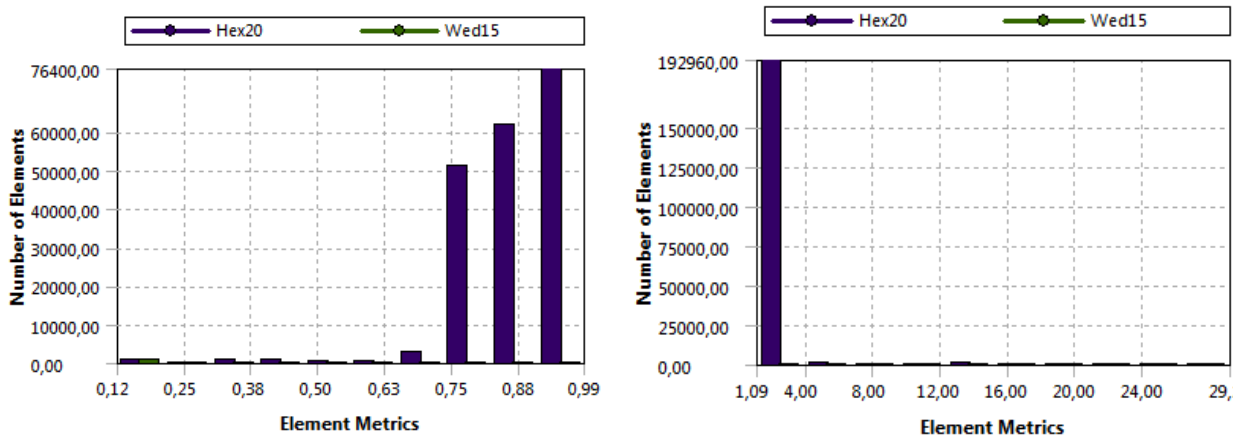

a) Element quality b) Aspect ratio

Figure 23. Element metrics of the previous mesh

The element quality average is 0,87 and the aspect ratio average is 1,88. There are few elements that have a high aspect ratio, but this is not worrisome, since they are few elements and located in areas of low stress. Such elements will not necessarily produce bad results – that depends on the loading and boundary conditions of the problem – but do introduce the potential for trouble.

4.3.2 Boundary conditions

The boundary conditions are other important aspects to comment before performing the static analysis since the results depend on its application.

First, the support of the rollers can be modeled as a fixed support, because this only allows the movement in the longitudinal axis (x-axis), on which loads do no act.

Second, the device's own weight has been considered, because it can have a significant influence on a 2 m cantilever. The mass of the device is 39,465 kg and the centroid in on x- axis (953,5 mm).

Finally, the loads generated by eddy currents calculated in the previous chapter are applied as point moments. The load of flexion in the small cylinder is totally negligible (16 $N \cdot m$) compared to the rest, but to be on the safety side it is joined with the loads applied to the larger cylinder. The torsion loads are applied on the centroins of each cylinder.

Figure 24 shows the boundary conditions on FILD

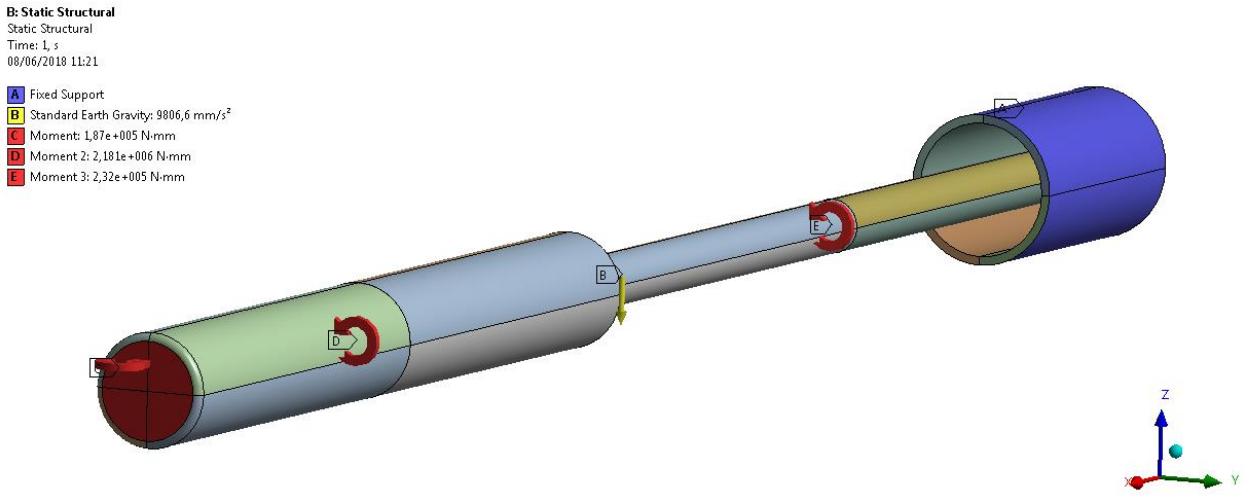

Figure 24. Boundary conditions in the structural static model

A good practice to check that the boundary conditions are well applied is to obtain the reactions in the fixed support. These results are shown in table 5.

Table 5. Force and moments reactions in the fixed support

Fx (N)	Fy (N)	Fz (N)	Mx ($N \cdot m$)	My ($N \cdot m$)	Mz ($N \cdot m$)
0	0	387	2413	369	187

The reaction forces on the x and y axes are zero and on the z-axis is the weight of FILD. On the other hand, the reaction moments of torsion (x axis) is equal to the sum of the moments applied, and the same happens with the flexion in the z-axis. There is also a moment in the y-axis due to the application of the weight in the center of gravity of FILD.

The obtained values coincide with the theoretical ones so the next step is to perform the static analysis.

4.3.3 Static structural analysis

In this section, once the mesh and the boundary conditions are explained, the results of the static analysis will be displayed.

To check the feasibility of the design, the results of the equivalent Von-Misses stress will be compared with the elastic limit of the material (270 MPa). Plasticity is an undesirable situation because it generates a permanent deformation that can affect the structural integrity and in addition to the measurement made. But the plasticity of small areas very localized is accepted as long as it does not compromise the entire section.

Figure 25 shows the stress distribution in FILD. In this figure, cross sections are shown because the predominant effect is the torsion that generates the same tension on the surface but varies in thickness. With a cross section it can be seen a representation of the stress variation.

There are two conflicting zones that are potential stress concentrators. The union of cylinder 1 (larger cylinder) and cylinder 2 (smaller cylinder) and the union of cylinder 2 with the roller support. These zones will be analyzed in detail and shown in figure 25 b – c.

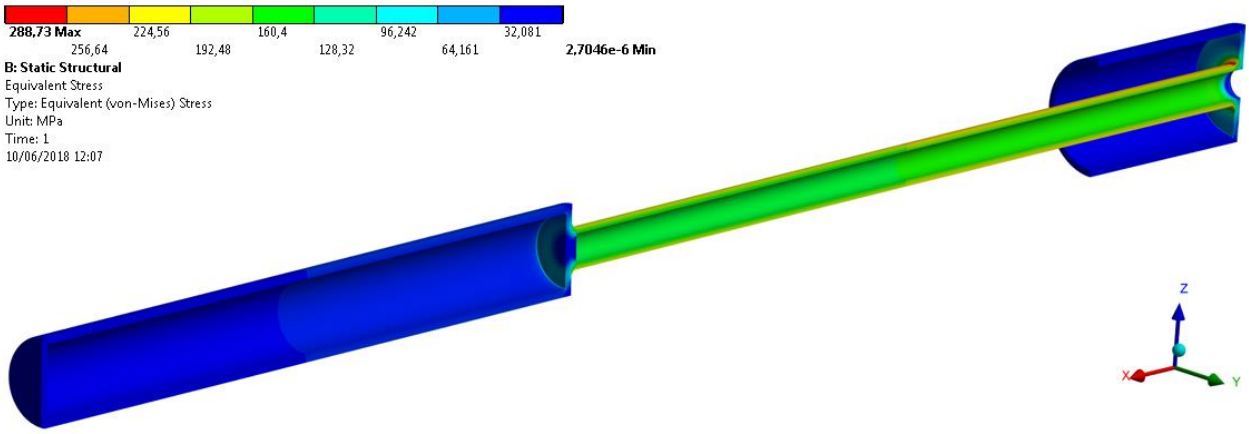

a) Stress distribution in FILD (general view)

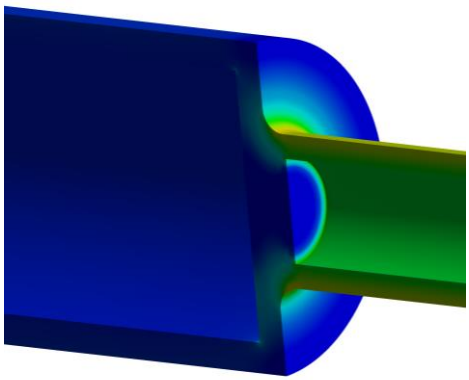

b) Stress in the stress concentrator 1

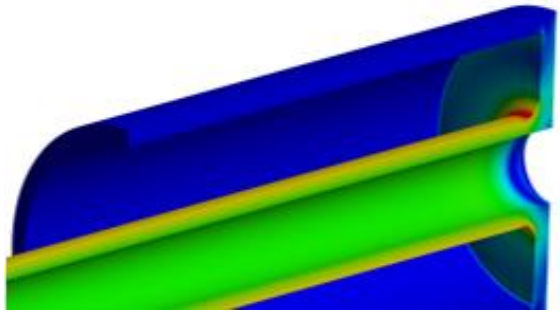

c) Stress in the stress concentrator 2

Figure 25. Stress distribution in FILD

The first conclusion that is obtained from this figure is that there is plastification because the maximum stress is 288,73 MPa that occurs in the stress concentrator 2.

In general, it can be seen that cylinder 1, as is logical, hardly supports stress due to its greater diameter and therefore greater inertia. However, cylinder 2 (smaller), is exposed to a stress around 224 MPa on its surface.

In the stress concentrator 1 (Figure 25 – b) there is no problem because the stress simply varies between the value of cylinder 1 and cylinder 2 and does not increase.

In the stress concentrator 2 (Figure 25 – c) the same does not happen. Due to the proximity to the support and after a cantilever of 2 meters, the stress is concentrated in a localized area. This zone will be the one that limits the design, although if it is in a localized area, the only thing that would happen wild be a small superficial plastification in the stress concentrator and a hardening by deformation.

Another interesting aspect is to verify that there are no excessive deformations. Figure 26 shows the total deformations in FILD.

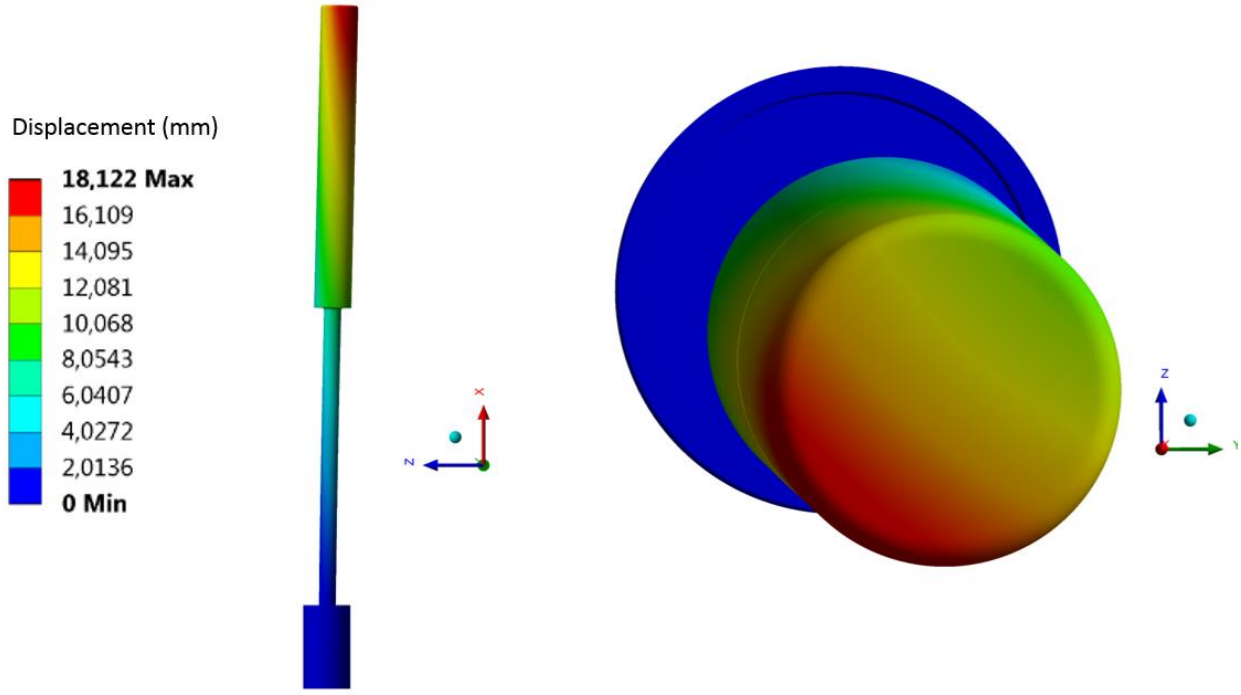

a) Total deformation (toroidal view) b) Total deformation (radial view)

Figure 26. Total deformation in FILD

The total deformation generated especially by the torsion torque and the own weight reaches a peak of 18,12 mm.

Because this state is inadmissible, it is necessary to change the current design to obtain a result in which stresses and deformations are adequate, without the conceptual design being substantially modified.

Before modifying the design, it is important to verify the mesh used in the previous case. To do this, a sensitivity analysis of the mesh is performed, varying the number of elements and checking the value of the maximum equivalent Von-Misses stress (Figure 27).

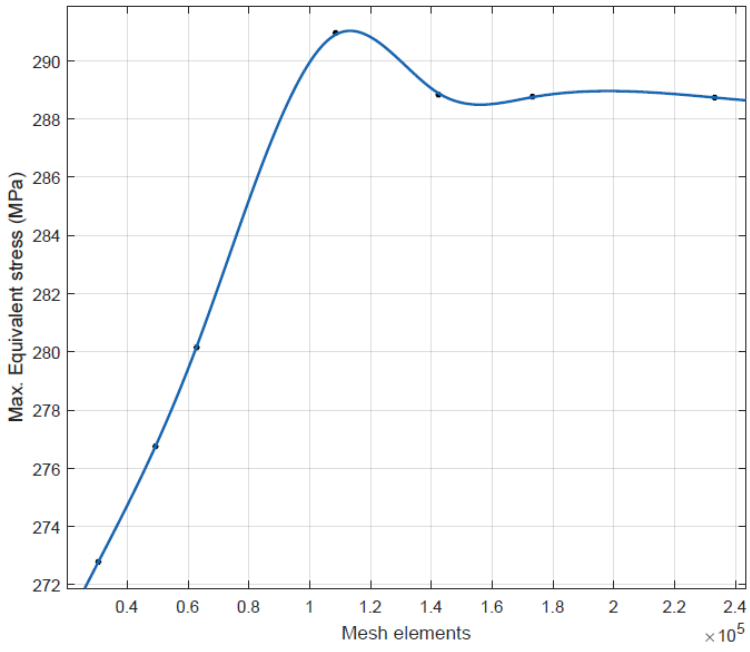

Figure 27. Sensitivity analysis of the mesh.

This analysis has been done by varying the number of elements between approximately 30000 elements and 230000.

In this graph, it can be observed, as expected, an increase in the maximum stress as the number of elements increases and finally the convergence around a value of 288,7 MPa. This is why the mesh used for the previous analysis is valid and will be used for the following ones.

In addition, to complete this analysis the variation of the stress along the thickness has been studied in the area where it is maximum, at the beginning of the rounding of the stress concentrator.

By varying the size of the mesh, it is intended to validate the result along the thickness. This is important because a very high stress on the surface may be acceptable if plastification does not occur in the entire section.

This analysis has been carried out taking into account the last three meshes of the sensitivity analysis, when the maximum stress value has already stabilized. The data of the meshes are the following:

- Mesh 1: 233100 elements / 1134358 nodes.
- Mesh 2: 173204 elements / 861634 nodes.
- Mesh 3: 142272 elements / 718220 nodes.

Figure 28 shows the stress-length (along the thickness) curves for the previously described meshes.

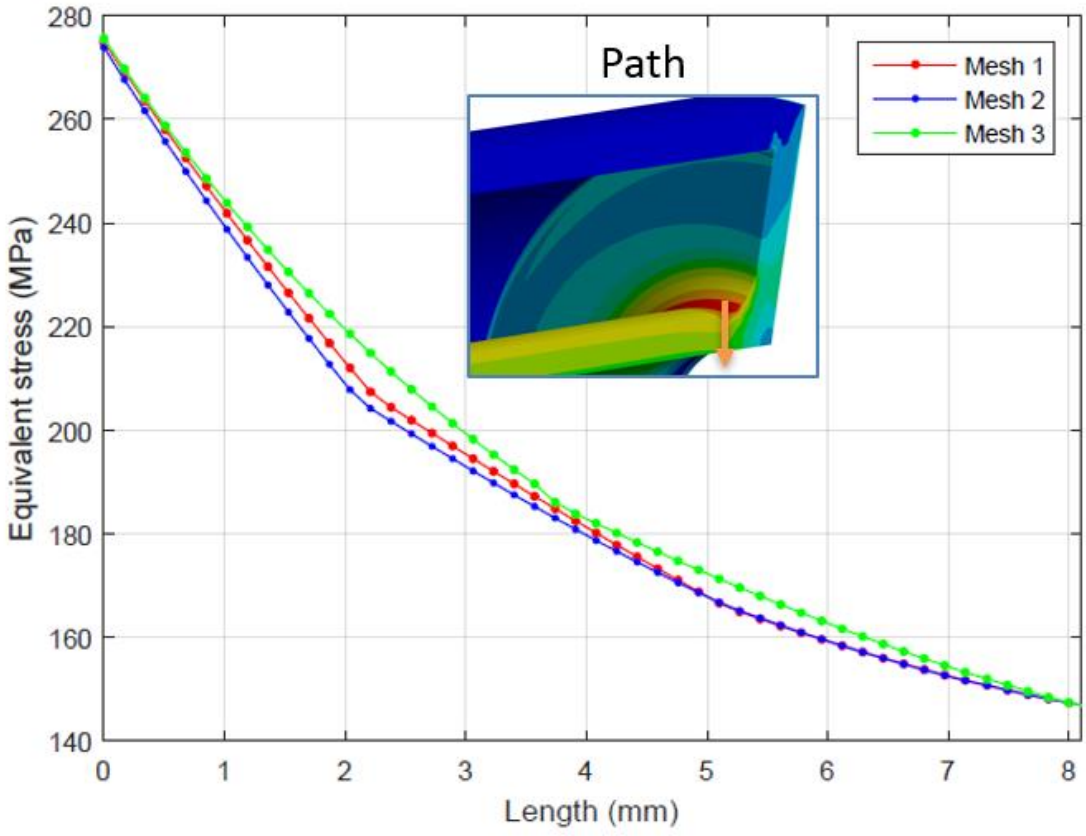

Figure 28. Equivalent stress vs length in thickness. Comparative between several meshes.

In this figure it can be seen that the results are very similar for the different meshes so it can be concluded that the mesh used previously not only calculates correctly the maximum equivalent stress, but also the stresses along the thickness.

In addition, an important fact that can be extracted from this graph is that only the first 0.5 mm (approximately) of the thickness (8 mm) are plastified in said region.

Once these checks are made, the next step is to make changes in the design optimally so that the stresses are below the elastic limit and get less deformations.

To make these necessary changes in an optimal way, an ANSYS tool called response surface has been used. This tool is capable of starting from one or several input parameters, establishing several design points, adjusting one or several output variables by means of a curve or surface.

Translating this idea to the FILD model, the output variable is clear, the maximum equivalent stress. To select the input parameters, variables that increase the inertia of the cylinder 2 have been used as criteria. Therefore, the variables selected to perform the parametric analysis are the outer radius and the thickness of the cylinder 2.

These variables have been assigned a range within which the tool normally offers 10 design points. In this case to better capture the response has been modified to 20 design points and the variables oscillating in the following range:

- Larger radius: Between 25 mm (conceptual design) and 35 mm.
- Thickness: Between 8 mm (conceptual design) and 15 mm.

The result is a 3D surface where the x-axis is the largest radius, the y-axis the thickness and the z-axis the maximum equivalent stress (Figure 29).

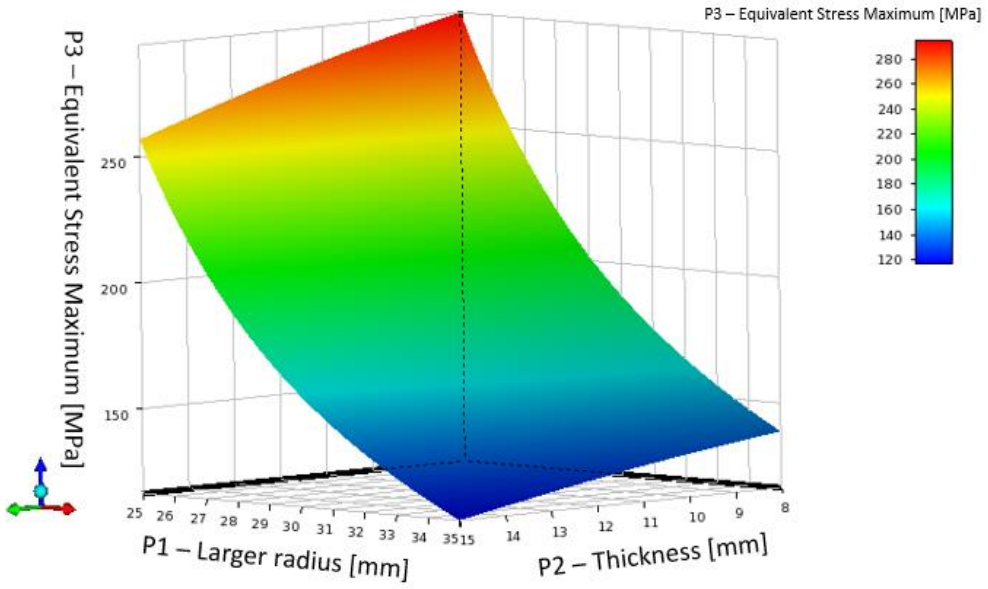

Figure 29. Equivalent stress maximum response surface versus larger radius and thickness.

A consequence of observing the previous figure is that the increase in the greater radius decreases more the maximum equivalent stress than the increase of thickness. So, the most decisive is to increase the radius.

Another aspect that can be visually extracted is that many of the different configurations are below the elastic limit (270 MPa). So, the goal now is to get as little as possible to modify the conceptual design so as not to exceed the elastic limit.

First, the option to modify the thickness is rejected, since it has little influence.

Second, modify the radius by interpolations of the previous curve to obtain an optimal result. These interpolations are made with ANSYS, which, like a 3D curve, can show a curve with the only influence of the greater radius. In this curve maximum stress – greater radius; the optimal point is sought.

As a result of these interpolations it is obtained that a radius of 30 mm can provide a good behavior increasing this dimension only 5 mm.

The expected result is only an interpolation, so to be sure that the behavior is as expected is necessary to perform

the static analysis with these conditions.

The results of the equivalent Von-Misses stress are shown in Figure 30.

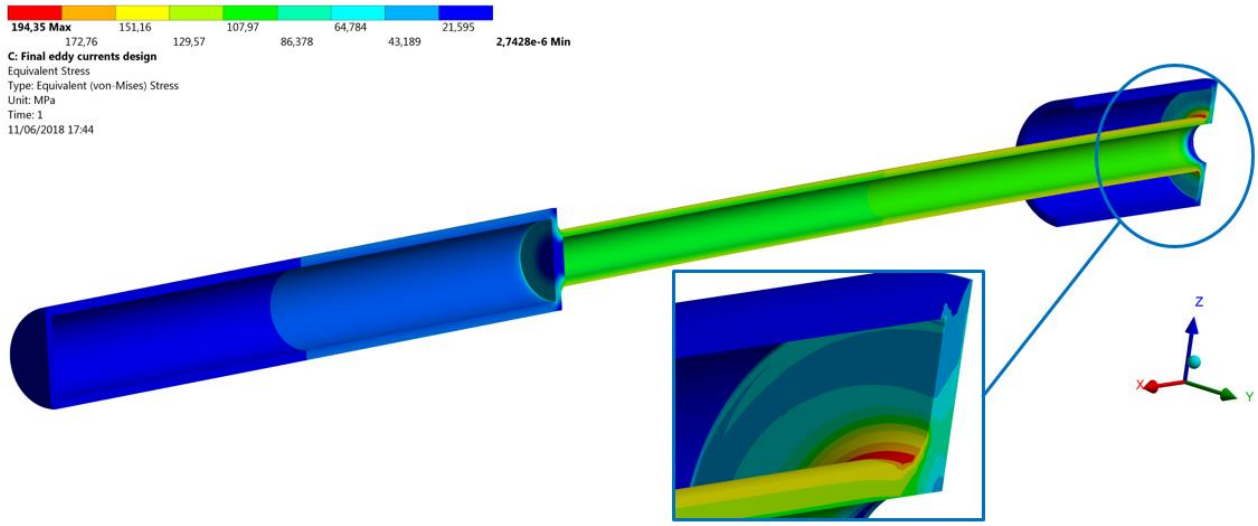

Figure 30. Stress distribution in FILD (Proposed design)

As can be seen in the previous figure, the maximum stress has decreased to below 200 MPa with only an increase of 5 mm radius.

Not only the maximum stress in the stress concentrator has decreased, but in the cylinder 2 the stresses are in a range between 100 and 150 MPa (approximately).

This result is good for structural integrity because with a proposed change of 16,7% in the radius of cylinder 2, the maximum stress has been reduced by 32,7%, leaving it totally out of risk of entering the plastic zone.

To complete the comparison between the conceptual and proposed design, Figure 31 shows the total deformation results in FILD both in toroidal view (Figure 31 – a) and in radial view (Figure 31 – b).

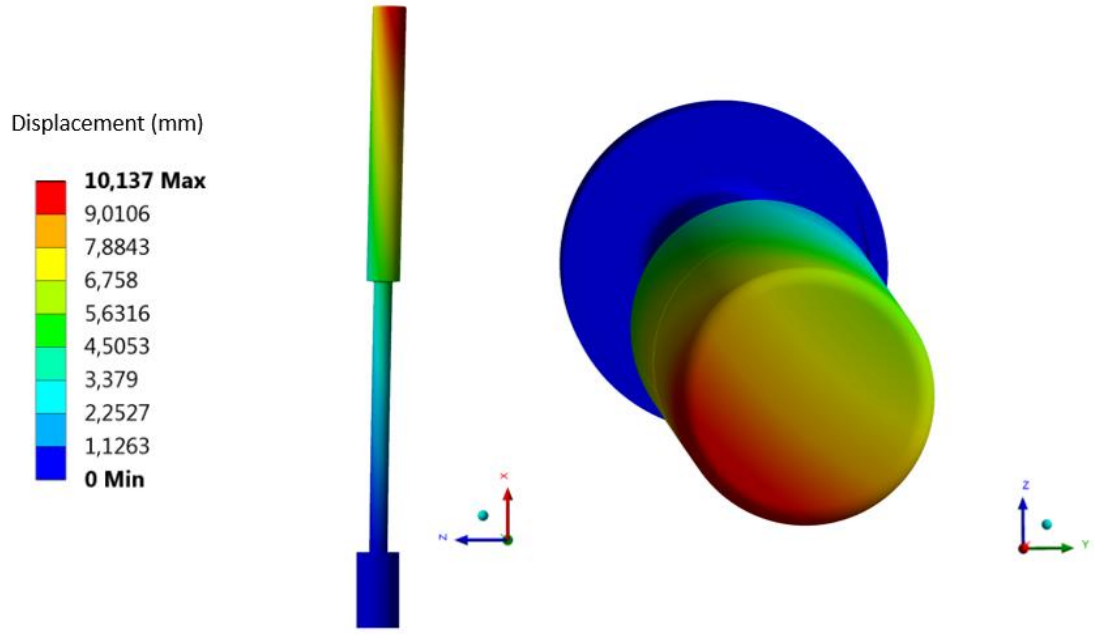

a) Total deformation (toroidal view) b) Total deformation (radial view)

Figure 31. Total deformation in FILD (Proposed design)

The results of the total deformations are also favorable. With this change, the maximum deformation has been reduced by almost 50%.

A deformation of 1 cm is totally acceptable and normal in this type of devices. In fact, in the preliminary design of the Upper Launcher (PBS 52.U#. P) similar deformations are obtained [21].

4.4 Halo current loads analysis

In this section the static analysis of FILD will be carried out to ensure the structural integrity against of the loads generated by Halo currents.

Then, the different aspects of the model (meshing, boundary conditions) will be discussed before commenting on the results.

Before going into detail explaining the mesh and the boundary conditions, it is necessary to explain an important detail of this load case. The loads calculated in chapter 3 for Halo currents, a distributed load of a value of 14,4 kN/m, are so large that they generate stresses that indicate that the device is not capable of supporting this load (approximately 9000 MPa).

Given this result, making changes in the design, as in the previous section, does not provide any substantial advantage that causes the stresses to approach the elastic limit.

Therefore, the solution proposed is to take into account the fixed part to reinforce the system, so that when FILD is deformed, there is a contact that helps resist stresses. This contact will be made through a ring on the body of FILD. Figure 32 shows the geometry of the fixed part and the contact ring.

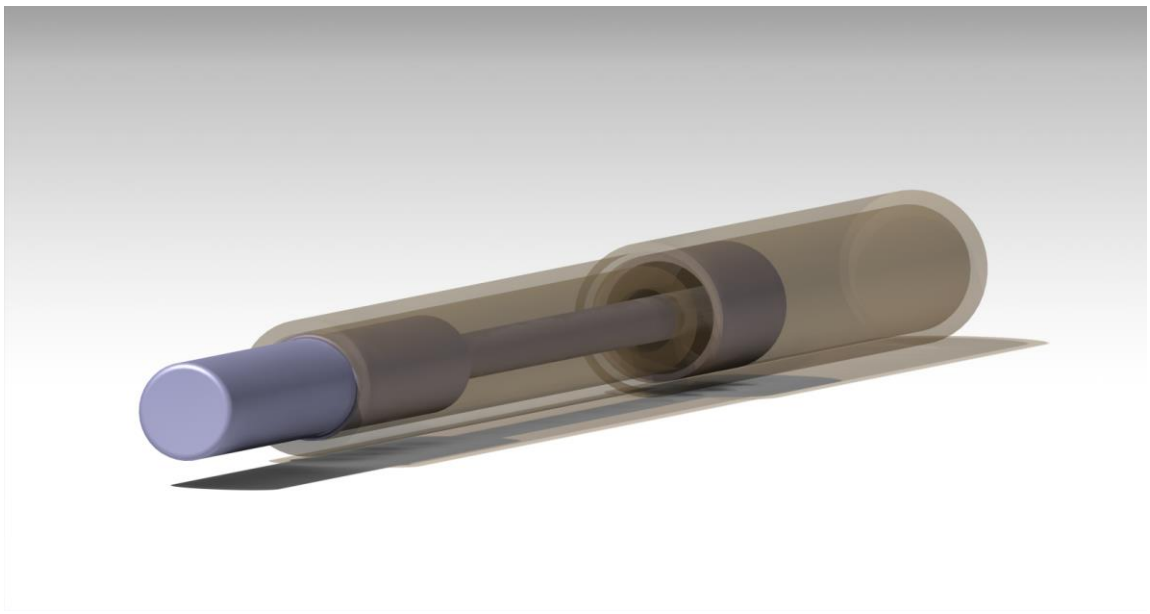

a) FILD CAD model general view

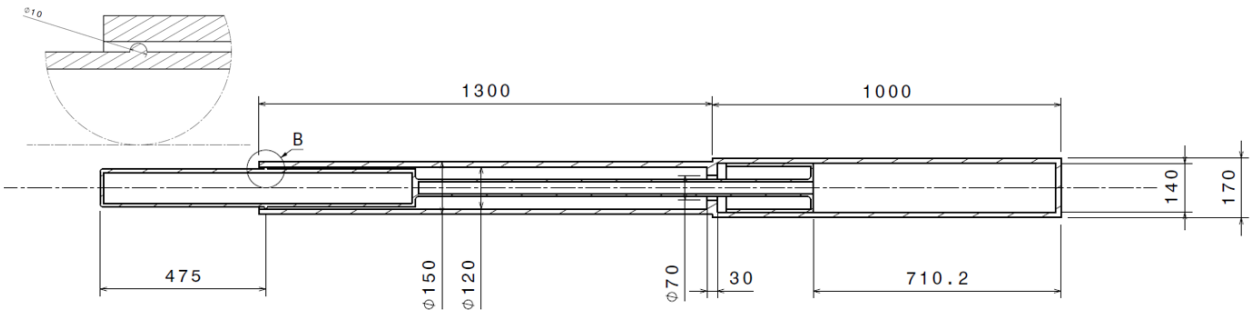

b) Cross section in the medium plane. Units in mm.

Figure 32. FILD CAD model (with fixed part)

This change in the model brings with it several consequences, among which is the existence of a contact that makes the problem non-linear and modeling the union of the movable and fixed part. This is explained in the boundary conditions, but before it is important to describe the mesh.

4.4.1 Mesh

Including the fixed part in the model means that the mesh is made for this part. The meshing philosophy is the same as in the previous section, using hexahedral elements.

On the other hand, the strategy is different, mainly due to the existence of a non-linear contact problem. If the mesh was a very important aspect in the analysis of the previous section (linear), in a non-linear problem it is much more, not only for capturing the result properly, but also for the convergence to a solution. In addition, computing time is increased by the use of iterative methods.

For these reasons, the meshing strategy has been the following:

- Use a large mesh size on the fixed part. The results in this part are not the main object of study, so knowing exactly the stress distribution in this element would increase the computational cost.
- Refine the mesh size in the stress concentrator 2. It is known that the most conflictive area is the stress concentrator; therefore, a finer mesh has been used in this place to correctly capture the maximum stress.
- A medium mesh size for the rest of the body of FILD. To speed up the calculation time, without giving up a good result.

Figure 33 shows the type of mesh used in this model (61933 elements).

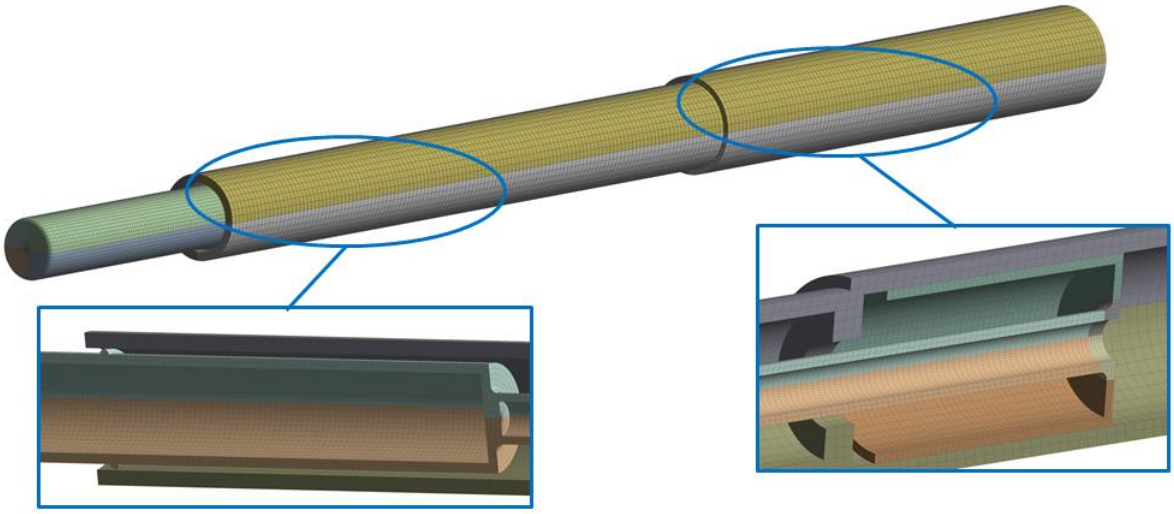

Figure 33. Mesh in Halo current model.

In spite of this optimization of the mesh, a sensitivity analysis will be carried out to improve the computing time.

To complete the information, the parameters of element quality and aspect ratio of the previously exposed mesh are shown in figure 34.

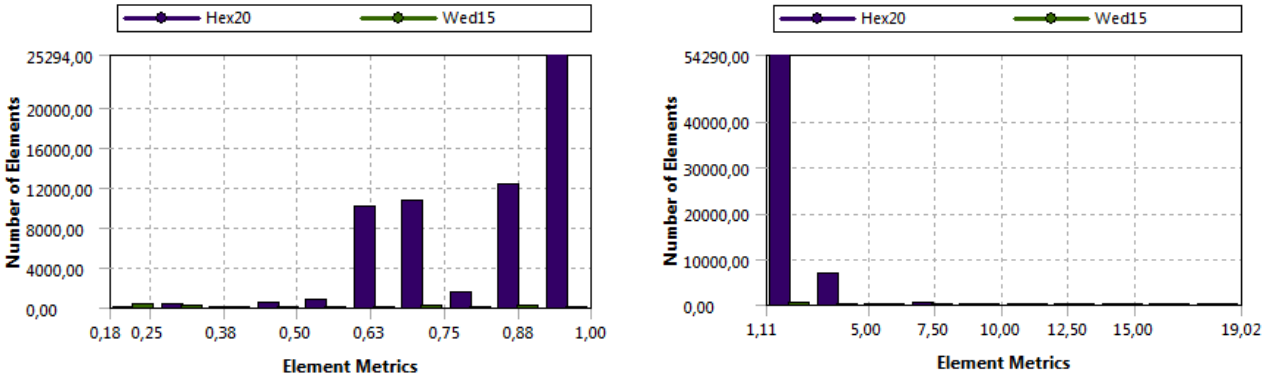

a) Element quality b) Aspect ratio

Figure 34. Element metrics of the previous mesh

The element quality average is 0,83 and the aspect ratio average is 1,96. The result is similar to the mesh proposed in eddy currents analysis, but with fewer elements, thanks to its optimization.

4.4.2 Boundary conditions

The boundary conditions have changed substantially with respect to the static analysis of loads caused by eddy currents, mainly the union of the movable part with the fixed part, but also the modeling of the contact between the ring and the fixed part.

Union between movable and fixed part

This union is materialized by means of rollers anchored to the FILD base, so as to allow axial movement rolling on the fixed part.

Due to the fact that the design is in a conceptual phase, the rollers and their axes have not been modeled yet so that for static analysis it is considered that the fixed and movable part are joined in the area of the rollers. In ANSYS there is this type of contact and it is called bonded contact.

If contact regions are bonded, then no sliding or separation between faces or edges is allowed. This type of contact allows for a linear solution since the contact length/area will not change during the application of the load.

The relative position between the two parts has been made for the measurement position that is when FILD receives the loads by Halo current.

Contact between the contact ring and fixed part

The contact between the fixed part and the contact ring included in the FILD body complicates the resolution of the model due to the existence of a static non-linear problem.

The non-linearity comes from the fact that initially the parts are not in contact, but as the FILD body deforms, it reaches a point where the two bodies come into contact, modifying the stiffness of the system.

That is why this contact has been modeled using the Frictionless type. This setting models standard unilateral contact; that is, normal pressure equals zero if separation occurs. Thus, gaps can form in the model between bodies depending on the loading. This solution is nonlinear because the area of contact may change as the load is applied. A zero coefficient of friction is assumed, thus allowing free sliding. In these analyzes a significant influence of the friction between the faces is not expected.

Non-linearity of problems can come from various causes: Non-linear material, geometric non-linearity due to large displacements, changes in boundary conditions, etc. One of the most problematic for convergence is the

contact, for this reason there are three basic aspects of the definition of contact that have not been controlled by computer:

- Contact formulation. An Augmented Lagrange formulation has been chosen. The finite contact Force, F_n, is a concept of contact stiffness, k_{Normal}. The higher the contact stiffness, the lower penetration, x_p, as illustrated in figure 35.

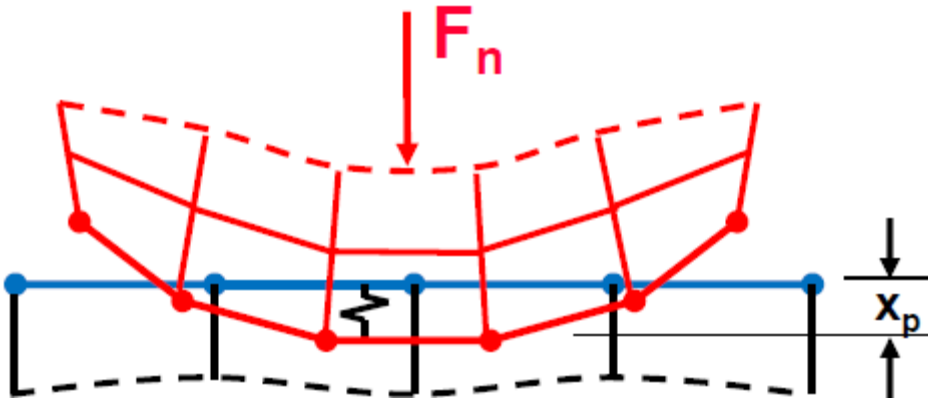

Figure 35. Augmented Lagrange formulation scheme

The augmented Lagrange formulation is:

$$F_n = k_{Normal} \cdot x_{Penetration} + \lambda$$

Because of the extra term λ, the Augmented Lagrange method is less sensitive to the magnitude of the contact stiffness k_{Normal} [26]. This fact improves the convergence to a solution remarkably as it has been verified in different analyzes.

- Time step control. Time step controls offers an additional layer of convergence enhancement that allows bisections and adjustments to time step size based on changes in contact behavior. In this study, the predict for impact method has been used. Contact behavior is reviewed at the end of each substep to determinate whether excessive penetration or drastic changes in contact status have occurred. If so, the current substep is re-evaluated using a "bisected" time increment [27].

  In addition, this option predicts the minimal time increment needed to detect future changes in contact status (Figure 36 – right). This is important since in the current model, there is an initial gap, which subsequently closes and changes the contact status.

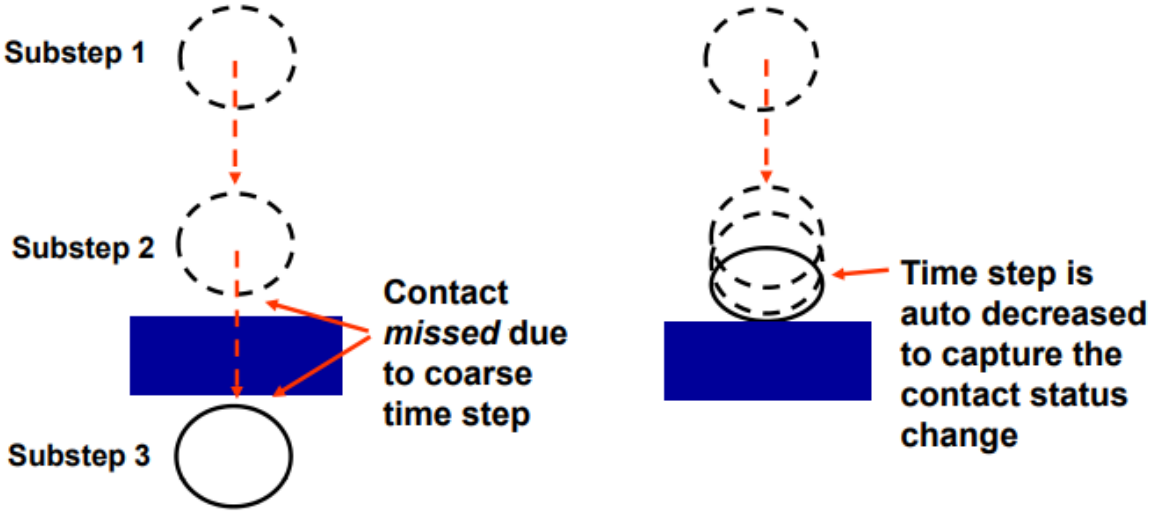

Figure 36. Time step controls. Bisection method (left), Predict for impact (right).

- Large deformations. Due to the high loads that act on FILD, the deformations that appear can be considered that they are not in the range of small deformations. By activating this mode, ANSYS uses a formulation suitable for large displacements and therefore improves convergence.

On the other hand, the load has been applied along FILD, and has been employed in several loading steps (normally three steps, two small and one with full load). In addition, in the first step, it has been necessary to calculate several substeps to correctly detect the impact.

In figure 37 the boundary conditions imposed in the model are shown.

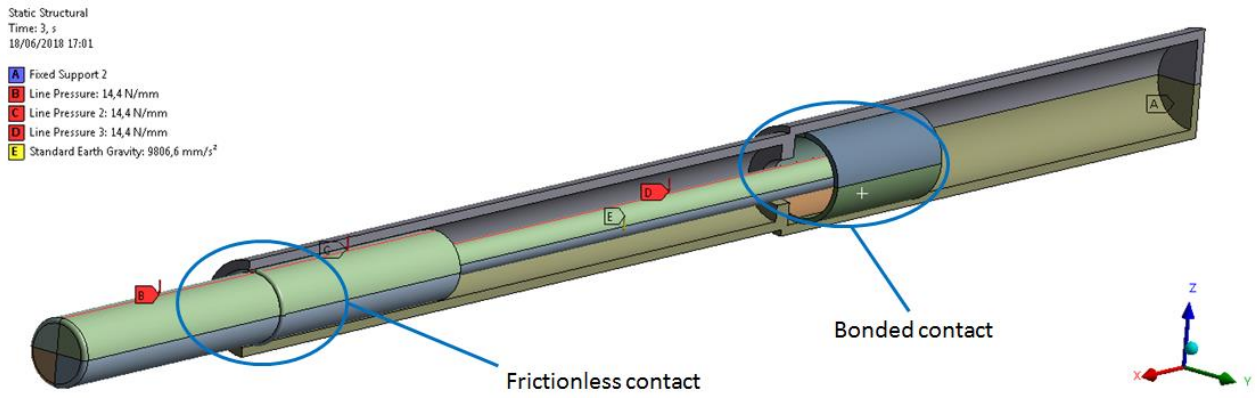

Figure 37. Boundary conditions in Halo current model

To check the correct application of the boundary conditions, table 6 shows the forces and moments of reaction on the support of the fixed part.

Table 6. Force and moment reactions in Halo current model

Fx (kN)	Fy (kN)	Fz (kN)	Mx ($kN \cdot m$)	My ($kN \cdot m$)	Mz ($kN \cdot m$)
0	0	30,464	0	52,094	0

The only loads that apply (own weight and Halo current load) occur in the z-direction, so there is only one force in the z axis and one moment in the y axis.

It can be easily verified that the resulting values correspond to the theoretical ones. The sum of the own weight (164 kg) and the load distributed along FILD provides the force value in the z-axis. The moment in the y-axis can be calculated as the sum of the moment that generates the own weight applied to the centroid and the corresponding moment generated by the loads distributed in the fixed support.

4.4.3 Static structural analysis

In this section, the necessary static analyzes will be performed to obtain an acceptable structural integrity due to Halo current loads.

As explained above, the design of FILD by itself or by realizing changes that do not affect the concept, is not able withstand the stresses that appear due to these loads. Therefore, the results will be presented taking into account the fixed part and the contact ring.

Initially the contact ring was placed at such distance that it was at the edge of the fixed part (in measuring position). In figure 38 the results of this first analysis are shown.

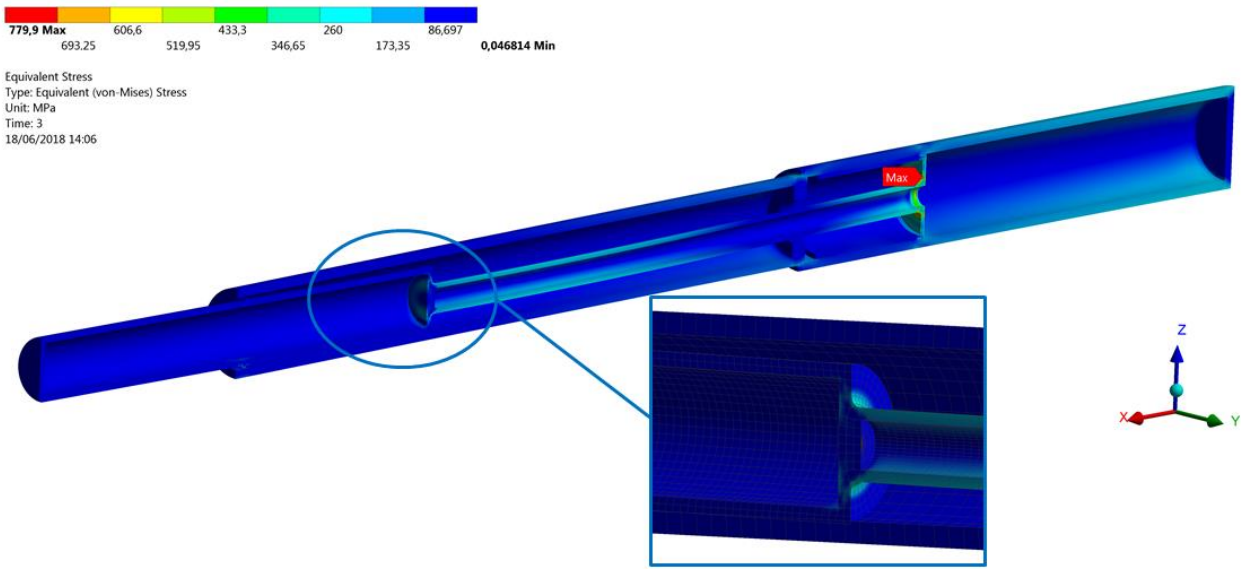

Figure 38. Equivalent stress in FILD (conceptual phase). Detail of the penetration.

The deformation of FILD shows a typical curvature of the bi-supported beams, which is the objective of placing the contact ring.

However, as it can be seen in the figure 38, the stresses are still excessive and located in the stress concentrator 2 (about 780 MPa).

In addition, a contact occurs in an area not intended or desired, at the end of the head support. This is because when the contact between the ring and the fixed part is established, the span is so large that the flexion causes the displacement in the head support to reach the fixed part in this area.

These two facts are totally inadmissible in the design, since they indicate the total structural failure of the device.

To solve mainly the problem of unwanted contact, but also the excessive stresses, the concept of bi-supported beam was used. By reducing the span between the two supports, stresses can be reduced; taking into account that the section of the probe head is cantilevered.

To observe this behavior, a parametric analysis has been performed in which the distance of the contact ring to the probe head is varied, reducing the distance between supports. In the conceptual design, the distance between the probe head and the ring is 475 mm, therefore, the range of variation is between 600 mm and 800 mm.

Since this analysis requires the calculation of several points and given the high computational cost that is assumed with the non-linear problem, the calculations have been made with a coarse mesh in order to obtain the behavior of the stress and its optimal point.

Figure 39 shows the behavior curve of the maximum equivalent stress versus the distance of the contact ring to the probe head.

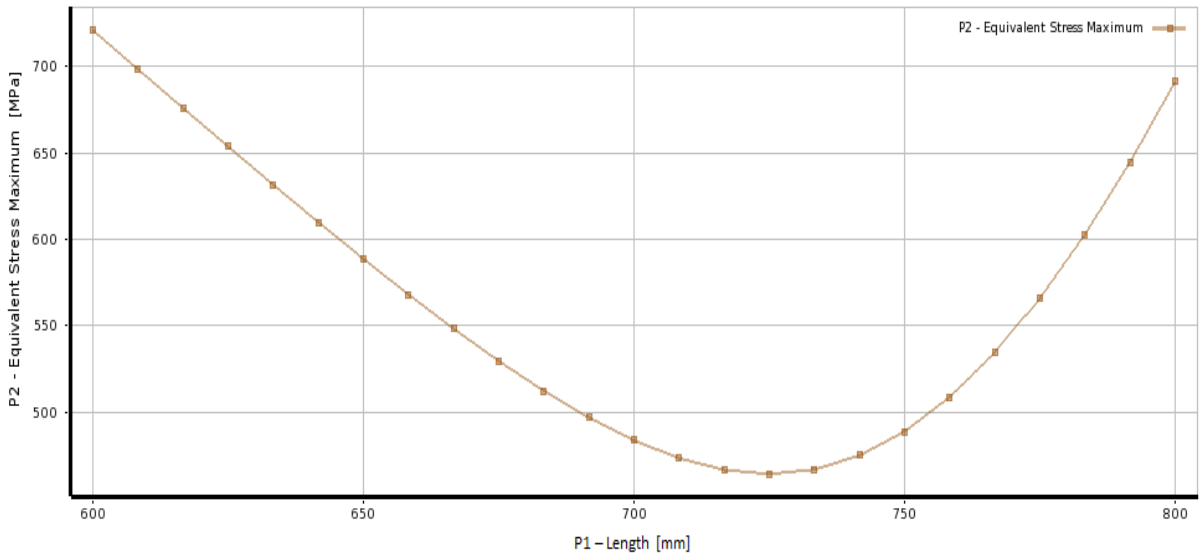

Figure 39. Equivalent stress maximum vs length between the contact ring and the probe head

It can be seen that the maximum equivalent stress decreases when the span is reduced, until it reaches a minimum. Subsequently it increases possibly caused by an excessively large overhang in the part of the probe head.

The optimum point that is obtained in the minimum of the curve is for a length of 725 mm. With this configuration, it is expected to obtain a stress result around 450 MPa, approximately half that in the previous case.

To validate this result, a static study was carried out with the contact ring in the optimum situation, with a dense mesh, as the one described in section 4.4.1.

Figure 40 shows the general distribution of stresses as well as details of the points of greatest interest.

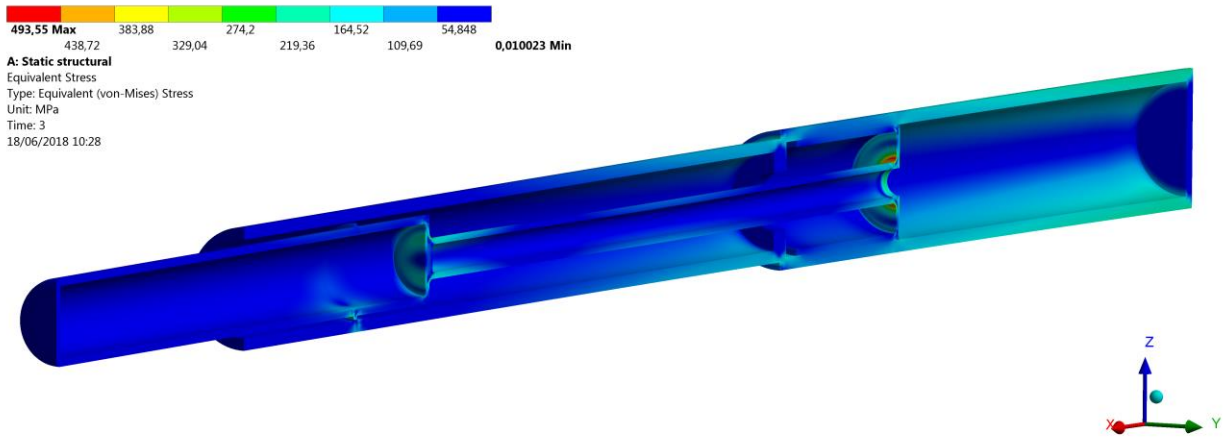

a) Stress distribution in FILD (General view)

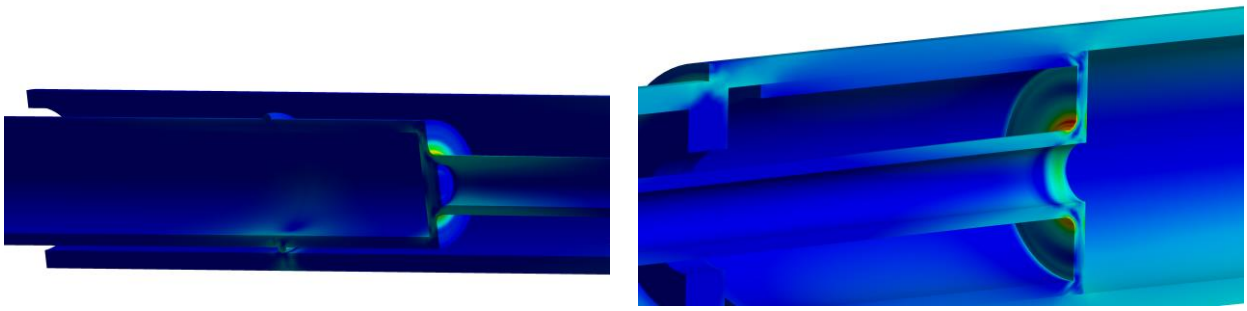

b) Detail of the contact and stress concentrator 1

c) Detail of the stress concentrator 2

Figure 40. Stress distribution in FILD (725 mm contact ring)

In these images it can be seen that there is no contact between unwanted parts, only in the contact ring. There are three points where stress can be a problem: the two stress concentrators, as in the previous analysis and the contact between the ring and the fixed part. The stress that occur in the contact area are not excessive and are overcome by stress concentrators.

The maximum stress is given in the stress concentrator 2 with a value of 493 MPa. This value is still not acceptable but it is one more step to avoid plastification. The deformations that occur in the z axis due to the flexion generated by the loads are also very high (Figure 41).

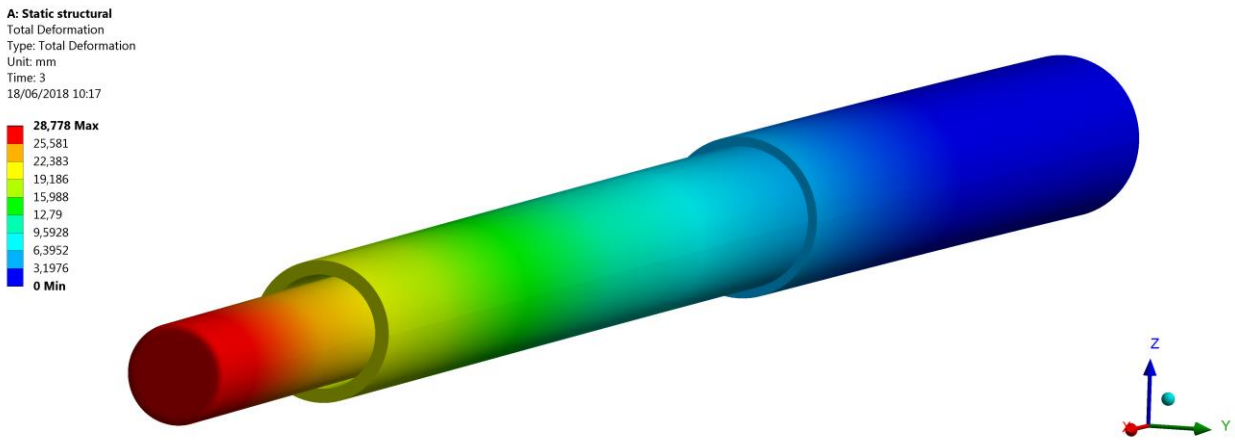

Figure 41. Deformation in FILD (725 mm contact ring)

Since a valid model has been obtained (there are no interferences between the parties) and due to the discrepancy between the result obtained in the parametric analysis, with a coarse mesh (~450 MPa) and in the last static analysis with a fine mesh (493,55 MPa), it is necessary to perform a sensitivity analysis of the mesh.

To achieve convergence with a lower number of elements (an important aspect because the calculation time can be increased excessively), as explained in the mesh section, a very refined mesh has been used in the stress concentrator 2 (where the maximum stress occurs).

The size of the mesh has been varied between 30000 and 80000 elements (approximately) to check the behavior of the maximum stress (Figure 42).

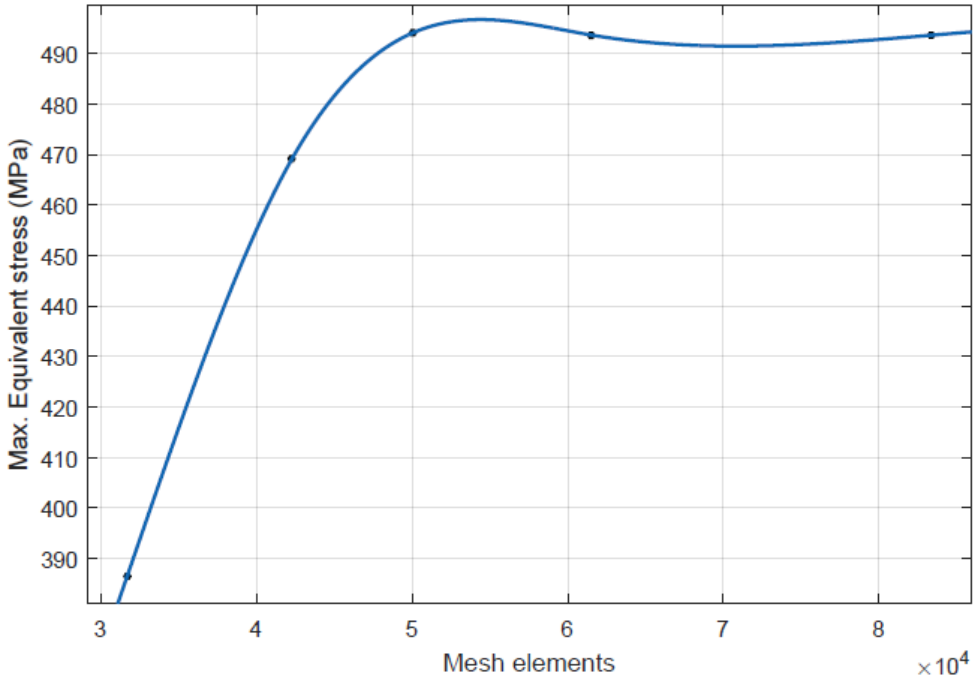

Figure 42. Sensitivity analysis of the mesh

From 50000 to 80000 elements approximately, there is a clear convergence in which the stress fluctuates around 1 MPa. The convergence is obtained for a smaller number of elements (with respect to the mesh of eddy currents model) thanks to the optimization of the mesh, with a very refined mesh in the stress concentrator, medium size in the body of FILD and large size in the fixed part.

With this result it is concluded that the mesh used in the last static analysis is valid because it is within the convergence range, although if a slightly thicker mesh is used it could decrease the calculation time and obtain a reliable result.

In order to continue with the design and that the device can resist the loads, the procedure outlined in the design of FILD in the case of eddy current loads is followed. In this case the only parameter to study is the outer radius, keeping the thickness fixed since it adds weight and does not influence as much as the radius.

Maintaining the same idea as in the contact ring analysis, the following study is based on studying the structural behavior of the system against changes in the external radius. A thick mesh will be used to capture the behavior, and then at the optimum point it is refined to obtain a valid result.

The variation range is between a radius of 25 mm (conceptual design) and 40 mm (maximum modification considered to not substantially change the conceptual design).

Figure 43 shows the results of this analysis.

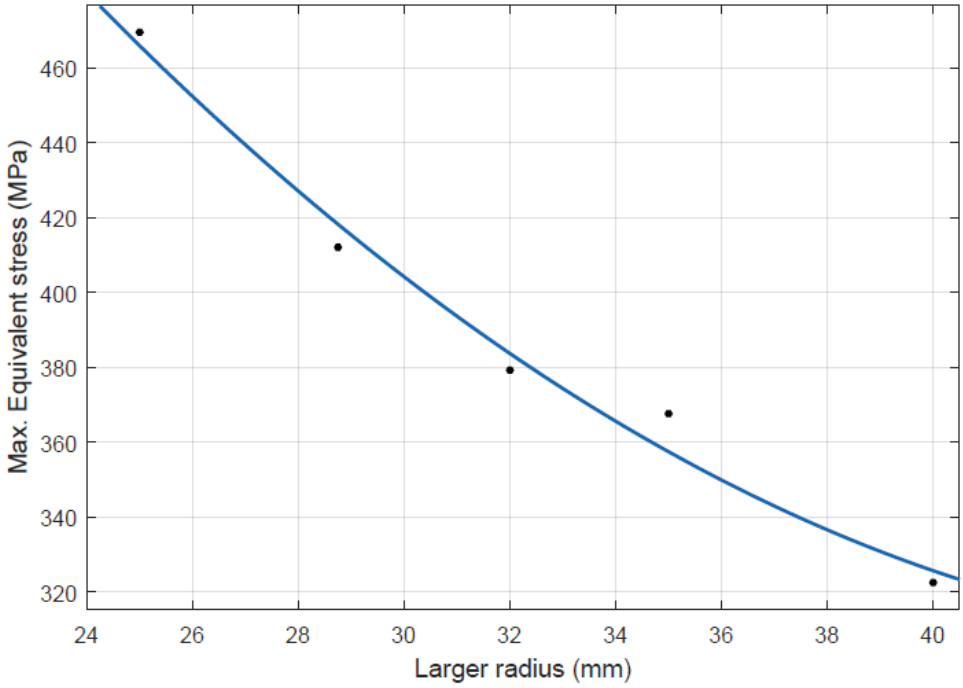

Figure 43. Equivalent stress maximum versus larger radius

The influence of the radius on the stresses that occur is completely clear since it increases the inertia of the weakest section. The decrease in the maximum stress between the conceptual design and the maximum radius value considered is approximately 30 %.

However, even for a radius of 40 mm the stresses that are expected are still excessive, around 320 MPa, but with a thick mesh, which when refined (entering the convergence zone) will be expected to be more stresses.

For these reasons, the outer radius is set at 40 mm to advance the design, but not complete it, because it is necessary to reduce more the stress.

To know exactly where the stresses occur and with what value a static analysis is made with a sufficiently fine mesh to be in the convergence zone (Figure 44).

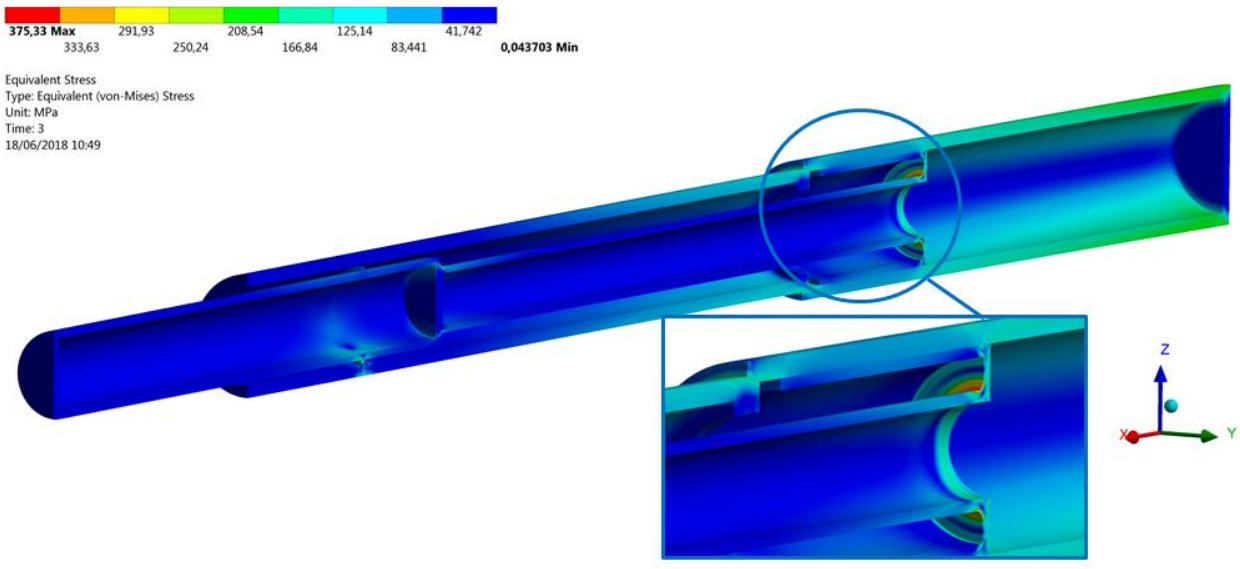

Figure 44. Stress distribution in FILD (40 mm larger radius)

Figure 44 shows a similar distribution of stresses with respect to the one obtained previously in the conceptual design, with the difference of a lower stress peak (375 MPa).

It should be noted that the stress in the contact as well as in the base of the support of the fixed part has increased its influence, but in no case it exceeds the stresses that occur in the stress concentrator 2 (only place where plastification exists).

Although the stress peak occurs in a very specific area, and not the entire section is plastified, it is convenient to reduce the stress in this area of conflict. For it, and because in general the stresses that appear on the body of FILD are very acceptable, the influence of parameters that reduce the stress in a localized way will be studied. These parameters are the following:

- Stress concentrator radius: This parameter is one of the most influential in the stress that is reached in a stress concentrator and still remains at a low value (7,5 mm) which can be increased to a maximum considered amount of 15 mm and observe the structural behavior.
- Thickness: The thickness of the area between the stress concentrator and the contact of the two parts can influence that there is a greater concentration of stresses in the curvature. In order to better distribute the stresses in this area, the increase in thickness from 8 mm to 15 mm will be studied.

This study is carried out by means of the response surface of the maximum stress (z-axis) in front of these two parameters (Figure 45).

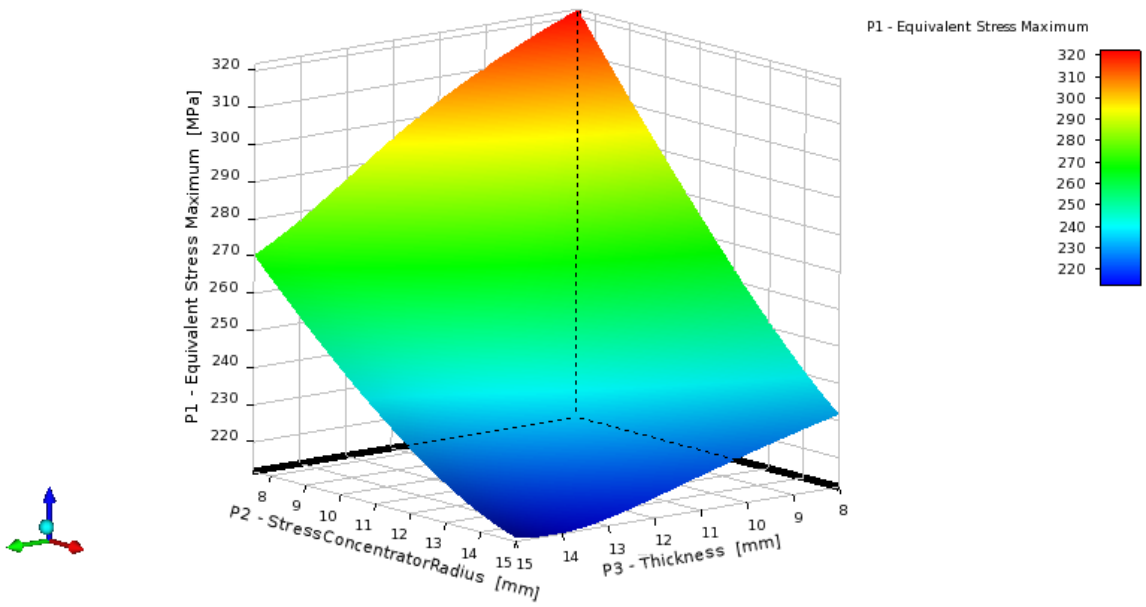

Figure 45. Equivalent stress maximum response surface versus stress concentrator radius and thickness.

The first consequence of this study is that it can be determined that the radius of the stress concentrator influences more than the thickness to reduce the stress. Another consequence is that a large part of the surface is below the 270 MPa limit.

Any point that could provide a maximum stress value of less than 270 MPa could be obtained, but because with little variation of the two parameters the result is much improved, the maximum value (15 mm) has been chosen for these variables (around 220 MPa of maximum equivalent stress).

Figure 46 shows the stress distribution for this configuration.

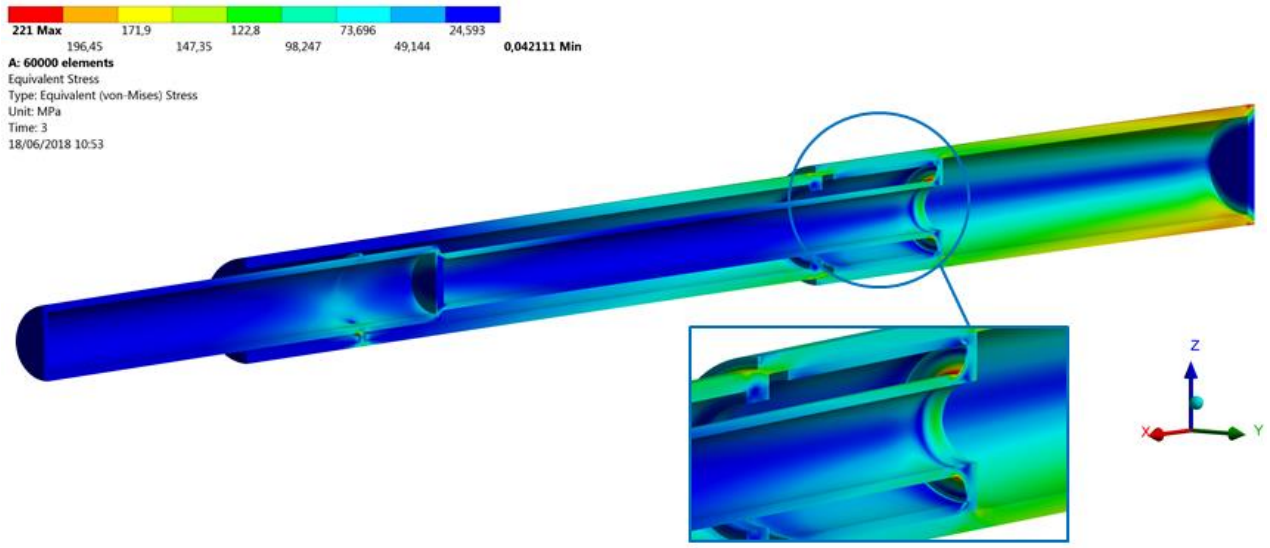

Figure 46. Stress distribution in the proposed final design

The simulation shows a peak stress of 221 MPa which is significantly below the critical $3S_m$ value of 270 MPa. It can be observed how the stress is distributed more in the contact and in the support of the fixed part.

Finally, a valid model has been obtained that supports the loads applied with a wide margin of safety to avoid plastification. But there is one final aspect to keep in mind:

The separation between the contact ring and the fixed part is 1 mm, while the own weight of FILD, in this last configuration generates a flexion of approximately 2 mm (Figure 47) which would cause a permanent contact which is not allowed because it exists relative movement in vacuum to change from the measurement position to a parking position (it is allowed in case of loads of Halo currents).

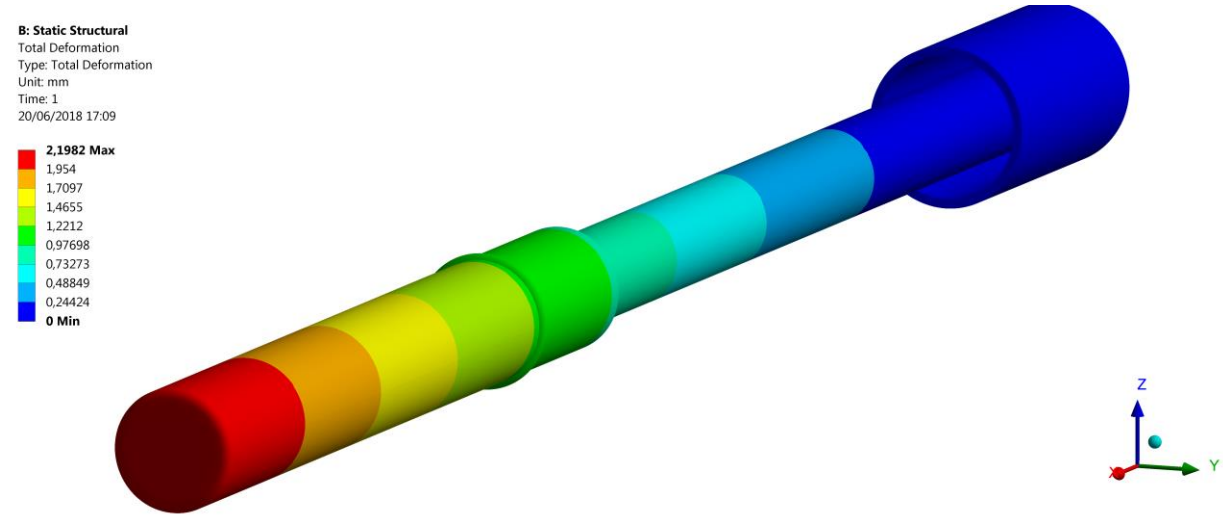

Figure 47. Deformation generated by own weight

To solve this problem, it is proposed to extend the diameter of the fixed part to a value greater than 2 mm, so that FILD's own weight does not cause permanent contact. Increasing the diameter leads to an increase in the stresses since there is a longer time when the loads are only supported by FILD, therefore a configuration is proposed so that there is a separation of 4 mm.

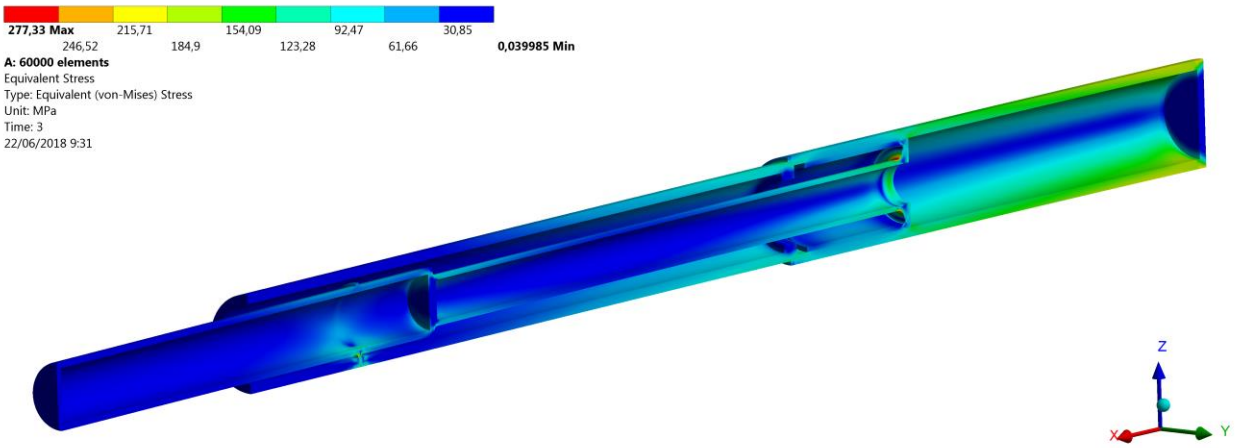

Figure 48. Stress distribution in proposed final design (Gap 4 mm)

In the previous figure it can be seen the distribution of stresses in this configuration. The peak stress that occurs in the voltage concentrator 2 is 277 MPa, so there is a small plastification in a very small and superficial area. For more detail in Figure 49 the most affected area is shown.

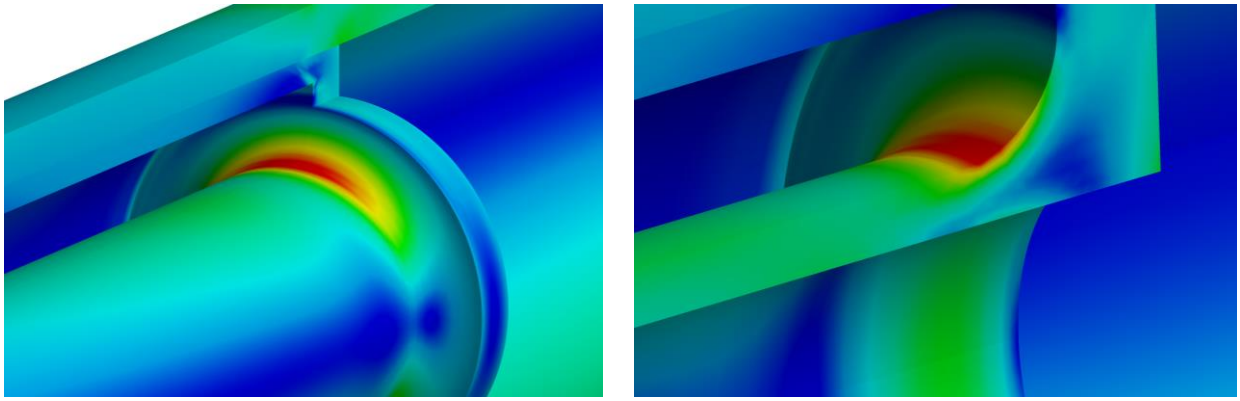

a) Detail 1 of the plastified zone b) Detail 2 of the plastified zone

Figure 49. Details of the plastified zone

Taking into account the low plastification value (Figure 48), the small plastic area (Figure 49 – a) and the little penetration in the thickness (Figure 49 – b), it can be concluded that the only phenomenon that can occur is a small permanent deformation at the surface level, which will also generate a hardening by deformation avoiding successive permanent deformations.

For these reasons, a valid design is considered structurally and functionally since it avoids the permanent contact generated by the own weight.

Finally, the deformations that occur in this model are shown in figure 50 below.

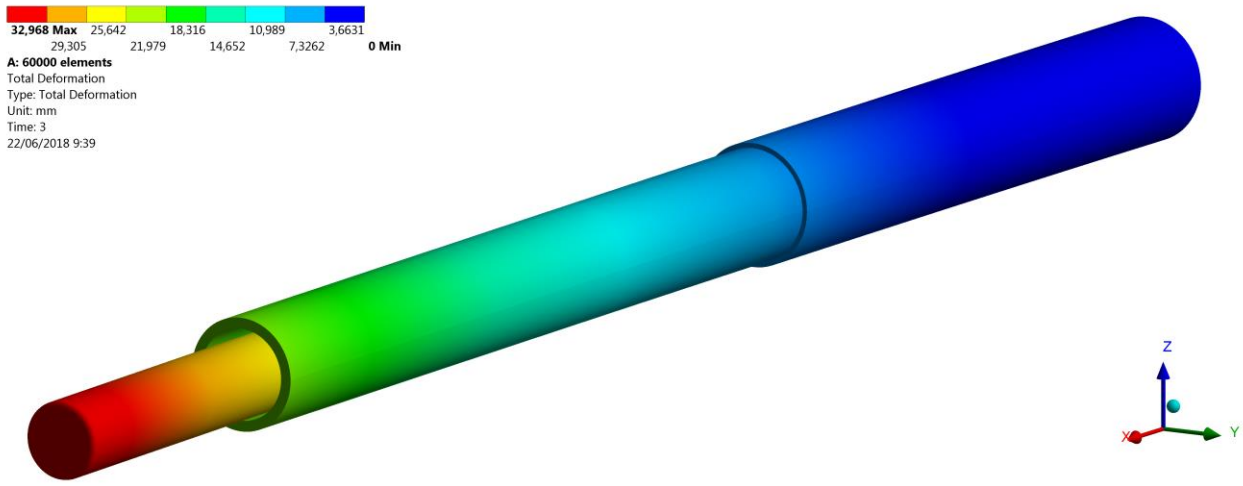

Figure 50. Deformation in proposed final design (Gap 4 mm)

The deformations that occur are large in general, with a peak of about 3 cm. But considering the value of the loads to which FILD is exposed and that it is a cantilever of 2 m, these deformations are considered admissible.

5 CONCLUSIONS

5.1 Conclusions

Starting from the objective of this master thesis, the structural design of FILD against the loads generated by electromagnetic disruptions in ITER, the following conclusions are obtained:

- A design capable of supporting the loads generated by Halo currents has been proposed modifying the conceptual design as little as possible. This design resist, in addition, the case of loading by eddy currents, less severe, since the final design proposed for Halo currents, includes the proposed design for the case of Eddy currents.
- A design is proposed not only with good structural integrity, but also functional. The permanent contact in vacuum is not allowed, so taking into account that the conceptual design of FILD deflects 15 mm and in the final design 2 mm by the own weight, has been solved increasing the slack between the movable and fixed part.
- Models have been generated to calculate induced electromotive force, induced intensity and applied moments in devices such as FILD. In addition, these models have been moved to another FILD currently being designed for the tokamak JT 60-SA (Japan).
- Throughout the development of this project, knowledge of the general operation of ITER, its components, diagnostic systems and, in particular FILD has been acquired. Another objective fulfilled is to understand the loads that act on internal components to develop the necessary models.
- The expansion of knowledge of the ANSYS tool, so important in the field of mechanical engineering and design, as well as the development of a simulation tool that can be adapted to future design easily.

5.2 Future works

ITER includes many restrictions and the design process is very complex. Currently the design is in conceptual phase so the estimates made are valid, but it is necessary to corroborate them with other methods. From this presented model, several lines of work are opened:

- Check the estimation of electromagnetic loads due to disruption events by obtaining a 3D map of forces (in an Equatorial Port Plug) and interpolating the model in this region. This map can be obtained from a previous solution of a dedicated electromagnetic analysis carried out by other groups, or by carrying out the study itself in the region of interest.
- Deepen the knowledge of Halo currents. There are conflicting opinions about the existence of Halo currents in this type of devices, one of the worst load case. In addition, more detailed studies can be carried out on the retraction system and if it is able to prevent Halo currents from entering FILD.
- Weight optimization. The weight of the set of the fixed and movable part is around 167 kg. It is an improvable weight for a cantilever of 2 m so an important aspect to investigate in the future is to realize a lightened design that properly supports the loads.
- Check the design in other loads cases. The proposed design correctly supports electromagnetic loads, but the same cannot be said about other cases of loads, such as seismic. So, to carry out an analysis of the proposed design in front of an earthquake, or movements of the Vacuum Vessel during a VDE would be an interesting work.

REFERENCES

[1] World Energy Council, "World Energy Scenarios 2016," 2016.

[2] U.S. Energy Information Administration, "International Energy Outlook 2017," 2017.

[3] J. Ongena et al, "Energy for Future Centuries: Will Fusion be an Inexhaustible, Safe, and Clean Energy Source?," *Fusion Science and Technology,* no. 45, pp. 3-14, 2004.

[4] Fusion For Energy, "Understanding Fusion," 2015. [Online]. Available: http://fusionforenergy.europa.eu/understandingfusion/. [Accessed 14 05 2018].

[5] J. Wesson, Tokamaks, Oxford: Oxford University Press, 2011.

[6] ITER, "ITER in a few lines," ITER, 2017. [Online]. Available: https://www.iter.org/proj/inafewlines. [Accessed 14 05 2018].

[7] J. F. R. Rodríguez, Implementation of a Fast-Ion Loss Detector in the MAST Upgrade Spherical Tokamak, Master Thesis, Sevilla: Universidad de Sevilla, 2017.

[8] M. Kocan et al, "The impact of the fast ion fluxes and thermal plasma loads on the design of the ITER fast ion loss detector," *JINST,* vol. 12, 2017.

[9] M. Rodriguez Ramos, "Calibración absoluta y aplicación de los detecctores de pérdidas de iones rápidos basados en maeriales centelleadores para dispositivos de fusión nuclear," Universidad de Sevilla, Sevilla, 2017.

[10] ITER, "The ITER tokamak. Vacuum Vessel," [Online]. Available: https://www.iter.org/mach/vacuumvessel. [Accessed 3 06 2018].

[11] ITER, "The ITER tokamak. Magnets," [Online]. Available: https://www.iter.org/mach/magnets. [Accessed 03 06 2018].

[12] ITER, "The ITER tokamak. Blanket," [Online]. Available: https://www.iter.org/mach/blanket. [Accessed 03 06 2018].

[13] ITER, "The ITER tokamak. Divertor," [Online]. Available: https://www.iter.org/mach/divertor. [Accessed 03 06 2018].

[14] J. Guirao, "Load_Spec_Modular_DSM_55.Eq#11," URA32W, 2017.

[15] J. Ayllon-Guerola et al, "Dynamic and thermal simulations of a fast-ion loss detector for ITER," *Fusion Engineering and Design,* 2017.

[16] M. Lehnen et al, "Disruptions in ITER and strategies for their control and mitigation," *Journal of Nuclear Materials,* vol. 463, pp. 39-48, 2015.

[17] J. Guirao, "SLS Tritium and Deposit Monitor (55.GC) System," QEVV3H, 2015.

[18] S. Iglesias, "Load Specification for 55.G8 Erosion and Deposition," L28Y6Z, 2015.

[19] Sannazzaro G., "Load Specifications (LS)," 222QGL, 2017.

[20] J. Guirao, "EM_Analysis_55.Eq#11/12," URBGMU, 2017.

[21] Karlsruhe Institute of Technology (KIT), "Upper Launcher Preliminary Design Review," 2YFSEA, 2009.

[22] M. Sugihara et al, "Disruption scenarios, their mitigation and operation window in ITER," *Nuclear Fusion,* vol. 47, pp. 337-352, 2007.

[23] M. Kocan, "Thermal plasma loads and Halo currents," T3EVTA, 2016.

[24] ITER, "Materials for the ITER vacuum vessel and in-vessel components - current status," 2010.

[25] J.B.J. Hegeman et al, "Tensile properties of explosively formed 316L(N)-IG stainless steel with and without an electron beam weld," *Journal of Nuclear Materials,* pp. 870-873, 2011.

[26] Sharcnet, "Contact Formulation Theory," [Online]. Available: https://www.sharcnet.ca/Software/Ansys/17.0/en-us/help/wb_sim/ds_contact_theory.html. [Accessed 18 06 18].

[27] ANSYS, "Lecture 3: Introduction to Contact," [Online]. Available: http://inside.mines.edu/~apetrell/ENME442/Labs/1301_ENME442_lab6_lecture.pdf. [Accessed 18 06 18].